

Oxygen and nitrogen abundances in nearby galaxies

Correlations between oxygen abundance and macroscopic properties

L.S. Pilyugin^{1,2}, José M. Vílchez², Thierry Contini³

¹ Main Astronomical Observatory of National Academy of Sciences of Ukraine, 27 Zabolotnogo str., 03680 Kiev, Ukraine (pilyugin@mao.kiev.ua)

² Instituto de Astrofísica de Andalucía, CSIC, Apdo, 3004, 18080 Granada, Spain (jvm@iaa.es)

³ Laboratoire d'Astrophysique de l'Observatoire Midi-Pyrénées – UMR 5572, 14 avenue E. Belin, 31400 Toulouse, France (contini@ast.obs-mip.fr)

Received 16 October 2003 / accepted 16 June 2004

Abstract. We performed a compilation of more than 1000 published spectra of H II regions in spiral galaxies. The oxygen and nitrogen abundances in each H II region were recomputed in a homogeneous way, using the P-method. The radial distributions of oxygen and nitrogen abundances were derived. The correlations between oxygen abundance and macroscopic properties are examined. We found that the oxygen abundance in spiral galaxies correlates with its luminosity, rotation velocity, and morphological type: the correlation with the rotation velocity may be slightly tighter. There is a significant difference between the luminosity – metallicity relationship obtained here and that based on the oxygen abundances determined through the R_{23} -calibrations. The oxygen abundance of NGC 5457 recently determined using direct measurements of T_e (Kennicutt, Bresolin & Garnett 2003) agrees with the luminosity – metallicity relationship derived in this paper, but is in conflict with the luminosity – metallicity relationship derived with the R_{23} -based oxygen abundances. The obtained luminosity – metallicity relation for spiral galaxies is compared to that for irregular galaxies. Our sample of galaxies shows evidence that the slope of the O/H – M_B relationship for spirals (-0.079 ± 0.018) is slightly more shallow than that for irregular galaxies (-0.139 ± 0.011). The effective oxygen yields were estimated for spiral and irregular galaxies. The effective oxygen yield increases with increasing luminosity from $M_B \sim -11$ to $M_B \sim -18$ (or with increasing rotation velocity from $V_{\text{rot}} \sim 10 \text{ km s}^{-1}$ to $V_{\text{rot}} \sim 100 \text{ km s}^{-1}$) and then remains approximately constant. Irregular galaxies from our sample have effective oxygen yields lowered by a factor of 3 at maximum, i.e. irregular galaxies usually keep at least 1/3 of the oxygen they manufactured during their evolution.

Key words. Galaxies: abundances - Galaxies: ISM - Galaxies: spiral - Galaxies: evolution

1. Introduction

Investigating the macroscopic properties of galaxies that could drive their chemical evolution is very important in understanding their global evolution, which has been the goal of many studies over the past twenty years. It has been found, for example, that the properties of H II regions in late-type galaxies are linked to macroscopic characteristics of galaxies such as luminosity or Hubble type. Smith (1975) concluded that excitation differences among the H II regions of Sbc–Scd–Irr galaxies can be best understood in terms of an abundance sequence which progresses from higher to lower heavy-element enrichment as one progresses from earlier to later type galaxies. He also noted that his results show no apparent correlation between the average heavy-element abundance and galaxy mass. The

correlation between oxygen abundance and the morphological type of galaxy was later confirmed by Vila-Costas & Edmunds (1992) and Zaritsky, Kennicutt & Huchra (1994).

Lequeux et al. (1979) revealed that the oxygen abundance correlates with total galaxy mass for irregular galaxies, in the sense that the higher the total mass, the higher the heavy element content. Since the galaxy mass is a poorly known parameter, the metallicity – luminosity relation instead of the mass – metallicity relation is usually considered (Skillman, Kennicutt & Hodge (1989); Richer & McCall (1995); Hunter & Hoffman (2000); Pilyugin (2001c); Melbourne & Salzer (2002), among others). Garnett & Shields (1987) found that spiral disk abundance also correlates very well with galaxy luminosity. They concluded that the metallicity of galaxies correlates better with galaxy luminosity than with morphological type. Zaritsky, Kennicutt & Huchra (1994) found that the

characteristic gas-phase abundances and luminosities of spiral galaxies are strongly correlated, and this relationship maps almost directly onto the luminosity – metallicity relationship of irregular galaxies.

The origin of this correlation is open to debate. It is widely suggested that there are two mechanisms which can be responsible for a luminosity – metallicity relation for spirals and irregulars: higher astration level and decreasing efficiency of heavy-element loss with increasing luminosity. The mass exchange between a galaxy and its environment can alter the relation between oxygen abundance and gas mass fraction; it mimics the variation in the oxygen yield. To investigate the possibility of a varying yield, Edmunds (1990) and Vila-Costa & Edmunds (1992) have suggested to use the “effective” oxygen yield, y_{eff} , as the yield that would be deduced if a system was assumed to behave as in the simplest model of chemical evolution. The variation of the value of the effective oxygen yield from galaxy to galaxy can be considered as indicative of the efficiency of mass exchange between galaxies and their environments. A similar approach, the concept of the oxygen abundance deficiency in the galaxy which is introduced as a deficiency of the oxygen abundance observed in the galaxy in comparison with the oxygen abundance predicted by the closed-box model for the same gas mass fraction, has been used by Pilyugin & Ferrini (1998; 2000a,b). The effective oxygen yields for a set of spiral and irregular galaxies were derived recently by Garnett (2002). He found that the value of effective oxygen yield is approximately constant, $y_{\text{eff}} = 0.0112$, for $V_{\text{rot}} > 150 \text{ km s}^{-1}$. The effective oxygen yield decreases by a factor of 10 – 20 from $V_{\text{rot}} \sim 300 \text{ km s}^{-1}$ to 5. This means that low-mass galaxies have lost the bulk of their manufactured oxygen, up to 90 – 95%.

Accurate abundance determinations are mandatory for such investigations. In H II regions, they can be derived from measurements of temperature-sensitive line ratios, such as $[\text{OIII}]\lambda\lambda 4959,5007/[\text{OIII}]\lambda 4363$. Unfortunately, in oxygen-rich H II regions, the temperature-sensitive lines such as $[\text{OIII}]\lambda 4363$ are often too weak to be detected. For such H II regions, abundance indicators based on more readily observable lines were suggested (Pagel et al. 1979; Alloin et al. 1979). The oxygen abundance indicator $R_{23} = ([\text{OII}]\lambda\lambda 3727,3729 + [\text{OIII}]\lambda\lambda 4959,5007)/\text{H}\beta$, suggested by Pagel et al. (1979), has found widespread acceptance and use for the oxygen abundance determination in H II regions where the temperature-sensitive lines are undetectable. Grids of photoionization models are often used to establish the relation between strong oxygen line intensities and oxygen abundances (Edmunds & Pagel 1984; McCall et al. 1985; Dopita & Evans 1986; Kobulnicky et al. 1999; Kewley & Dopita 2002; among others). Radial distributions of oxygen abundance determined with theoretical (or model) calibrations have been obtained for large samples of spiral galaxies by Vila-Costas & Edmunds (1992), Zaritsky et al. (1994), van Zee et al. (1998), Considère et al. (2000), among others.

The early calibrations were one-dimensional (Edmunds & Pagel 1984; McCall et al. 1985; Dopita & Evans 1986; Zaritsky et al. 1994), i.e. a relation of the type $O/H = f(R_{23})$ was used. It has been shown (Pilyugin 2000; 2001a,b) that the error in the oxygen abundance derived with the one-dimensional calibrations involves a systematic error. The origin of this systematic error is evident. In a general case, the intensity of oxygen emission lines in spectra of H II regions depends not only on the oxygen abundance but also on the physical conditions (hardness of the ionizing radiation and geometrical factors) in the ionized gas. Thus, when one estimates the oxygen abundance from emission line intensities, the physical conditions in H II regions should be taken into account. In the T_e – method this is done via the electron temperature T_e . In one-dimensional calibrations the physical conditions in H II regions are ignored. Starting from the idea of McGaugh (1991) that the strong oxygen lines contain the necessary information for determining accurate abundances in (low-metallicity) H II regions, it has been shown (Pilyugin 2000; 2001a,b) that the physical conditions in H II regions can be estimated and taken into account via the excitation parameter P . A two-dimensional or parametric calibration (the so-called “P – method”) has been suggested. A more general relation of the type $O/H = f(P, R_{23})$ is used in the P – method, compared with the relation of the type $O/H = f(R_{23})$ used in one-dimensional calibrations. Thus, the one-dimensional R_{23} – calibration provides more or less realistic oxygen abundances in high-excitation H II regions, but yields overestimated oxygen abundances in low-excitation H II regions. This is in agreement with the results of Kinkel & Rosa (1994), Castellanos et al. (2002), Kennicutt, Bresolin & Garnett (2003), Garnett, Kennicutt & Bresolin (2004), who found that the R_{23} – method yields overestimated oxygen abundances in high-metallicity H II regions.

It should be stressed that “strong lines – oxygen abundance” calibrations do not form an uniform family. The calibrations of the first type are the empirical calibrations, established on the basis of H II regions in which the oxygen abundances are determined through the T_e – method. Two-dimensional empirical calibrations both at low and high metallicities were recently derived by Pilyugin (2000; 2001a,c). The calibrations of the second type are the theoretical (or model) calibrations, established on the basis of the grids of photoionization models of H II regions. The two-dimensional theoretical calibrations were recently proposed by Kobulnicky et al. (1999) and Kewley & Dopita (2002). It has been shown (Pilyugin 2003b) that there is a discrepancy between the oxygen abundances in high-metallicity H II regions determined with the T_e – method (and/or with the corresponding “strong lines – oxygen abundance” calibration) and that determined with the model fitting (and/or with the corresponding “strong lines – oxygen abundance” calibration). Thus, so far, there actually exist two scales of oxygen abundances in H II regions. The first (empirical) scale corresponds to the oxygen abundances derived with the T_e –

method or with empirical calibrations (the P – method). The second (theoretical or model) scale corresponds to the oxygen abundances derived through model fitting or with theoretical (model) calibrations.

Pilyugin (2003b) suggested to use the interstellar oxygen abundance in the solar vicinity, derived with very high precision from the high-resolution observations of the weak interstellar OI λ 1356 absorption line towards the stars, as a “Rosetta Stone” to make a choice between “theoretical” and “empirical” scales of oxygen abundances in high-metallicity H II regions. The agreement between the value of the oxygen abundance at the solar galactocentric distance traced by the abundances derived in H II regions through the T_e – method and that derived from the interstellar absorption lines towards the stars is strong evidence that the classical T_e – method provides accurate oxygen abundances in H II regions, i.e. the “empirical” scale of oxygen abundances in high-metallicity H II regions is correct. Therefore, at high metallicities the “strong lines – oxygen abundance” calibrations must be based on the H II regions with the oxygen abundances derived through the T_e – method but not on the existing grids of models for H II regions.

The usual quantities: the oxygen and nitrogen abundance distributions in galaxies (Sect. 2), the correlations between oxygen abundance and macroscopic properties of galaxies (Sect. 3 and Sect. 4), and the estimation of effective oxygen yields and their variations among galaxies (Sect. 5) will be considered in this paper.

What is the novelty of our study? All previous investigations of these problems were carried out with the R_{23} -based oxygen abundances. Let us refer to the recent analysis and conclusion of B. Pagel who is the founder of the R_{23} – calibrations: “Starting from around 1980, the notorious R_{23} method has been the most widely used method for the oxygen abundance determination. Investigations since then have shown that our calibrations have overestimated oxygen abundances near solar. There is some promise in newly developed strong-line indices and especially in refinements of the R_{23} method (P – calibration). Until more of these refinements have been applied, abundances near and above solar have to be taken with a grain of salt” (Pagel 2003). For the present study, the oxygen and nitrogen abundances for a large sample of H II regions in late-type galaxies will be derived using a homogeneous method: the two-dimensional calibration (P – method). In Sect. 6, the oxygen abundances obtained here will be compared with the recently derived T_e -based oxygen abundances in the disk of the galaxy NGC 5457 (Kennicutt, Bresolin & Garnett 2003). The O/H – M_B relationship obtained here with the P-based oxygen abundances will be compared with the O/H – M_B relationship obtained recently by Garnett (2002) on the basis of oxygen abundances derived through the R_{23} – calibrations. The comparison between P-based, T_e -based, and R_{23} -based data provides an additional check of the P-based abundances and shows the difference between the P-based and R_{23} -based data.

2. The chemical abundances

2.1. The algorithm for oxygen and nitrogen abundances determination

The oxygen and nitrogen abundances in H II regions are derived in the following way. We adopt a two-zone model for the temperature structure within H II regions.

As the first step, the $(O/H)_P$ oxygen abundance in H II regions is determined with the expression suggested in Pilyugin (2001a)

$$12 + \log(O/H)_P = \frac{R_{23} + 54.2 + 59.45P + 7.31P^2}{6.07 + 6.71P + 0.37P^2 + 0.243R_{23}}, \quad (1)$$

where $R_{23} = R_2 + R_3$, $R_2 = I_{[OII]\lambda 3727 + \lambda 3729} / I_{H\beta}$, $R_3 = I_{[OIII]\lambda 4959 + \lambda 5007} / I_{H\beta}$, and $P = R_3 / R_{23}$.

Then, the electron temperatures within the [OIII] and [OII] zones are derived. For this purpose the expressions for the oxygen abundance determination from Pagel et al. (1992) and the $T_e([OII]) - T_e([OIII])$ relation from Garnett (1992) are used,

$$\frac{O}{H} = \frac{O^+}{H^+} + \frac{O^{++}}{H^+}, \quad (2)$$

$$12 + \log(O^{++}/H^+) = \log \frac{I_{[OIII]\lambda 4959 + \lambda 5007}}{I_{H\beta}} + 6.174 + \frac{1.251}{t_3} - 0.55 \log t_3, \quad (3)$$

$$12 + \log(O^+/H^+) = \log \frac{I_{[OII]\lambda 3726 + \lambda 3729}}{I_{H\beta}} + 5.890 + \frac{1.676}{t_2} - 0.40 \log t_2 + \log(1 + 1.35x), \quad (4)$$

$$x = 10^{-4} n_e t_2^{-1/2}, \quad (5)$$

where n_e is the electron density in cm^{-3} (we assume a constant value of $n_e = 100 \text{ cm}^{-3}$), $t_3 = t_{[OIII]}$ is the electron temperature within the [OIII] zone in units of 10^4K , $t_2 = t_{[OII]}$ is the electron temperature within the [OII] zone in units of 10^4K . The t_2 value is determined from the equation (Garnett 1992)

$$t_2 = 0.7 t_3 + 0.3. \quad (6)$$

Using the value of O/H derived from Eq.(1) and the measured emission line ratios, Eqs.(2) - (6) can be solved for $t_{[OII]}$ and $t_{[OIII]}$.

Assuming $t_2 = t_{[NII]} = t_{[OII]}$, the N/O abundance ratio in H II regions is determined from the expression (Pagel et al. 1992)

$$\log(N/O) = \log(N^+/O^+) = \log \frac{I_{[NII]\lambda 6548 + \lambda 6584}}{I_{[OII]\lambda 3726 + \lambda 3729}} + 0.307 - \frac{0.726}{t_2} - 0.02 \log t_2. \quad (7)$$

Table 1. The adopted and derived parameters of the radial oxygen abundance distributions in galaxies

galaxy	R_{25} arcmin	$12+\log(\text{O}/\text{H})_0$	gradient dex/ R_{25}	$\Delta\log(\text{O}/\text{H})$ dex	number of H II regions	references
NGC0224	102.07	8.76	-0.52	0.09	22	BKC82, BKG99, DK81
NGC0253	14.09	8.71	-0.54	0.10	9	WS83
NGC0300	11.19	8.49	-0.40	0.13	45	CPG97, DCL88, dORW83, EP84, PEB79, WS83
NGC0598	37.06	8.57	-0.20	0.08	41	BKG99, DTP87, GOS92, KA81, MRS85, P70, S71, S75, VPD98
NGC0628	5.36	8.68	-0.45	0.08	37	BKG99, FGW98, MRS85, vZSH98
NGC0753	1.32	8.82	-0.21	0.08	12	HBC96
NGC0925	5.48	8.51	-0.48	0.10	20	vZSH98, ZKH94
NGC1058	1.62	8.71	-0.32	0.04	6	FGW98
NGC1068	3.54	8.83	-0.26	0.03	9	OK93, vZSH98
NGC1232	3.71	8.73	-0.58	0.09	15	vZSH98
NGC1365	5.61	8.74	-0.70	0.14	53	AEL81, PEB79, RW97
NGC1637	2.04	8.67	0.02	0.11	14	vZSH98
NGC2403	11.45	8.52	-0.35	0.11	56	BKG99, GSP99, GSS97, FTP86, MRS85, S75, vZSH98
NGC2442	3.23	8.70	-0.17	0.05	8	R95
NGC2541	3.30	8.23	0.14	0.14	19	ZKH94
NGC2805	3.30	8.44	-0.26	0.11	17	vZSH98
NGC2835	3.62	8.31	-0.07	0.12	17	R95
NGC2841	4.06	9.12	-0.78	0.01	5	BKG99, OK93
NGC2903	6.29	8.94	-0.71	0.09	31	MRS85, vZSH98, ZKH94
NGC2997	5.00	8.66	-0.39	0.08	6	EP84, MRS85
NGC3031	13.77	8.69	-0.43	0.09	36	BKG99, GS87, OK93, SB84
NGC3184	3.71	8.97	-0.63	0.06	30	MRS85, vZSH98, ZKH94
NGC3198	4.26	8.69	-0.64	0.07	14	ZKH94
NGC3344	3.54	8.63	-0.48	0.09	15	MRS85, VEP88, ZKH94
NGC3351	3.79	8.90	-0.26	0.05	19	BK02, BKG99, MRS85, OK93
NGC3521	5.48	8.86	-0.93	0.06	9	ZKH94
NGC3621	6.74	8.55	-0.44	0.12	26	R95, ZKH94
NGC4254	2.81	8.94	-0.65	0.06	19	HPC94, MRS85, SSK91
NGC4258	9.31	8.57	-0.20	0.08	33	BKG99, C00, OK93, ZKH94
NGC4303	3.23	8.84	-0.72	0.10	22	HPL92, SSK91
NGC4321	3.79	8.86	-0.37	0.06	10	MRS85, SSK91
NGC4395	6.59	8.27	-0.02	0.08	16	MRS85, vZSH98
NGC4501	3.54	8.99	-0.52	0.07	5	SKS96
NGC4559	5.48	8.48	-0.38	0.13	20	ZKH94
NGC4571	1.86	8.90	-0.20	0.04	4	SKS96, SSK91
NGC4651	2.04	8.72	-0.64	0.06	6	SKS96
NGC4654	2.45	8.85	-0.77	0.06	7	SKS96
NGC4689	2.18	8.89	-0.41	0.08	5	SKS96, SSK91
NGC4713	1.35	8.71	-0.73	0.05	4	SKS96
NGC4725	5.34	9.01	-0.88	0.13	8	ZKH94
NGC4736	5.61	8.60	-0.26	0.05	16	BKG99, MRS85, OK93
NGC5033	5.36	9.06	-1.78	0.06	5	ZKH94
NGC5055	6.29	9.01	-0.83	0.07	5	MRS85
NGC5068	3.88	8.32	+0.08	0.12	23	MRS85, R95
NGC5194	5.61	8.92	-0.40	0.06	21	BKG99, DTV91, MRS85
NGC5236	6.59	8.79	-0.28	0.07	27	BK02, DTJ80, WS83
NGC5457	14.42	8.80	-0.88	0.09	65	GSP99, KG96, KR94, MRS85, RPT82, S71, S75, SS78, TPF89, vZSH98
NGC6384	3.38	8.90	-0.62	0.05	16	BK02, BKG99, OK93
NGC6744	10.21	9.00	-0.89	0.04	16	R95
NGC6946	8.30	8.70	-0.41	0.06	9	FGW98, MRS85
NGC7331	5.74	8.68	-0.48	0.04	12	BKG99, OK93, ZKH94
NGC7793	4.78	8.54	-0.50	0.07	22	EP84, MRS85, WS83
IC0342	22.33	8.85	-0.90	0.12	5	MRS85
IC5201	4.26	8.27	+0.09	0.14	11	R95

Alternatively, the value of t_3 can be derived from the following expression for $t_P = t_3$ (Pilyugin 2001a)

$$t_P = \frac{R_{23} + 3.09 + 7.05P + 2.87P^2}{9.90 + 11.86P + 7.05P^2 - 0.583R_{23}}. \quad (8)$$

Then the oxygen (and nitrogen) abundances $(O/H)_{t_P}$ can be determined from Eqs.(2)-(7) with $t_3=t_P$. The oxygen abundance $(O/H)_{t_P}$ is in good agreement with the value of $(O/H)_P$ (the differences between $(O/H)_{t_P}$ and $(O/H)_P$ are usually less than 0.03 dex, see Fig. 12 in Pilyugin 2001a). However, for H II regions in which most of the oxygen is in the O^+ stage, the value of $(O/H)_{t_P}$ is less reliable than the value of $(O/H)_P$.

2.2. Central abundances and radial gradients

A compilation of published spectra of H II regions in late-type galaxies has been carried out. Our list contains more than 1000 individual spectra of H II regions in 54 late-type galaxies. We performed an extensive compilation of spectra of H II regions from the literature but our collection does not pretend to be exhaustive. Only the galaxies with available spectra for at least four H II regions were taken into consideration. Using these spectrophotometric data and the algorithm described in the previous section, the oxygen and nitrogen abundances were derived for our sample of H II regions.

In investigations of the relationships between the oxygen abundances and the macroscopic properties of spiral galaxies, the concept of the characteristic oxygen abundance has been introduced: it is defined as the oxygen abundance in the disk at a predetermined galactocentric distance. Due to the presence of radial abundance gradients in the disks of spiral galaxies, the choice of the characteristic (or representative) value of the oxygen abundance in a galaxy is not trivial. The value of the oxygen abundance at the B -band effective (half-light) radius of the disk (Garnett & Shields 1987; Garnett 2002), the value of the central oxygen abundance extrapolated to zero radius from the radial abundance gradient (Vila-Costas & Edmunds 1992), the value of the oxygen abundance at $r = 0.4R_{25}$, where R_{25} is the isophotal (or photometric, or Holmberg) radius, (Zaritsky, Kennicutt & Huchra 1994), and the value of the oxygen abundance at one disk scale length from the nucleus (Garnett et al. 1997), have been used as the characteristic oxygen abundance in a galaxy. To estimate the characteristic oxygen abundance in spiral galaxies, the radial distribution of oxygen abundances within the galaxies should be established.

The radial oxygen abundance distribution in every galaxy is well fitted by the following equation:

$$12 + \log(O/H) = 12 + \log(O/H)_0 + C_{O/H} \times (R/R_{25}), \quad (9)$$

where $12 + \log(O/H)_0$ is the extrapolated central oxygen abundance, $C_{O/H}$ is the slope of the oxygen abundance gradient expressed in terms of dex/ R_{25} , and R/R_{25} is the fractional radius (the galactocentric distance normalized to the disk isophotal radius).

Table 2. List of references to Table 1.

abrev	source
AEL81	Alloin, Edmunds, Lindblad, et al. 1981
BK02	Bresolin & Kennicutt 2002
BKC82	Blair, Kirshner & Chevalier 1982
BKG99	Bresolin, Kennicutt & Garnett 1999
C00	Castellanos 2000
CPG97	Christensen, Petersen & Gammelgaard 1997
DCL88	Deharveng, Caplan, Lequeux, et al. 1988
DK81	Dennefeld & Kunth 1981
dORW83	d’Odorico, Rosa & Wampler 1983
DTJ80	Dufour, Talbot, Jensen, et al. 1980
DTP87	Diaz, Terlevich, Pagel, et al. 1987
DTV91	Diaz, Terlevich, Vílchez, et al. 1991
EP84	Edmunds & Pagel 1984
FGW98	Ferguson, Gallagher & Wyse 1998
FTP86	Fierro, Torres-Peimbert & Peimbert 1986
GOS92	Garnett, Odewanh, & Skillman 1992
GS87	Garnett & Shields 1987
GSP99	Garnett, Shields, Peimbert, et al. 1999
GSS97	Garnett, Shields, Skillman, et al. 1997
HBC96	Henry, Balkowski, Cayatte, et al. 1996
HPC94	Henry, Pagel & Chincarini 1994
HPL92	Henry, Pagel, Lasseter, et al. 1992
KA81	Kwitter & Aller 1981
KG96	Kennicutt & Garnett 1996
KR94	Kinkel & Rosa 1994
MRS85	McCall, Rybsky & Shields 1985
OK93	Oey & Kennicutt 1993
P70	Peimbert 1970
PEB79	Pagel, Edmunds, Blackwell, et al. 1979
R95	Ryder 1995
RPT82	Rayo, Peimbert & Torres-Peimbert 1982
RW97	Roy & Walsh 1997
S71	Searle 1971
S75	Smith 1975
SB84	Stauffer & Bothun 1984
SKS96	Skillman, Kennicutt, Shields, et al. 1996
SS78	Shields & Searle 1978
SSK91	Shields, Skillman & Kennicutt 1991
TPF89	Torres-Peimbert, Peimbert & Fierro 1989
VEP88	Vílchez, Edmunds & Pagel 1988
VPD88	Vílchez, Pagel, Diaz, et al. 1988
vZSH98	van Zee, Salzer, Haynes, et al. 1998
WS83	Webster & Smith 1983
ZKH94	Zaritsky, Kennicutt & Huchra 1994

The derived parameters of the oxygen abundance distributions are presented in Table 1. The name of the galaxy is listed in column 1. The isophotal radius R_{25} (in arcmin) taken from the Third Reference Catalog of Bright Galaxies (de Vaucouleurs et al. 1991) is given in column 2. The extrapolated central $12 + \log(O/H)_0$ oxygen abundance and the gradient (the coefficient $C_{O/H}$ in Eq.(9)) expressed in terms of dex/ R_{25} are listed in columns 3 and 4. The scatter of oxygen abundances around the general radial oxygen abundance trend is reported in column 5. The number of available individual spectra of H II regions in the galaxy is listed in column 6. The source(s) for the

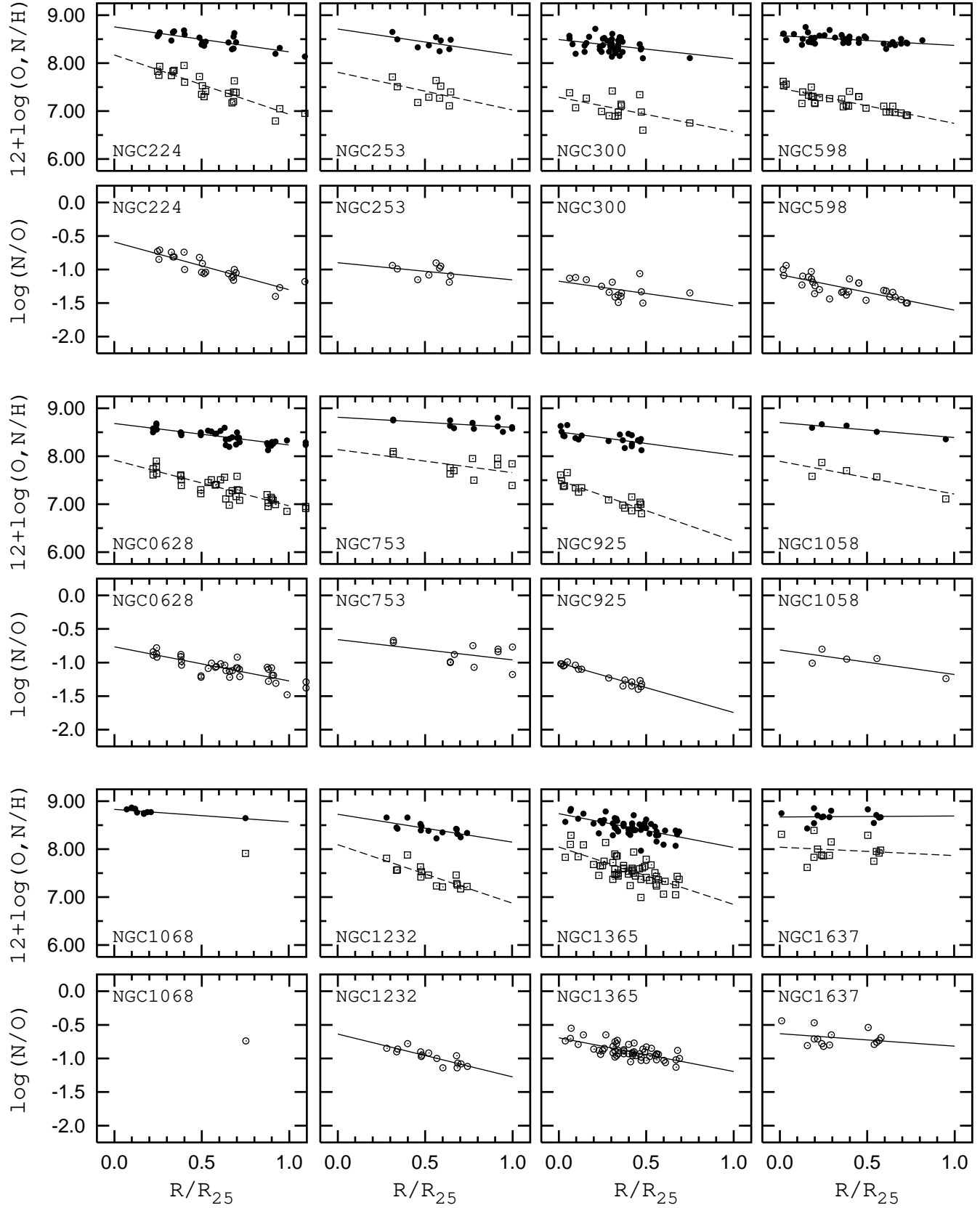


Fig. 1. Oxygen and nitrogen abundances, and nitrogen-to-oxygen abundance ratios versus galactocentric distance for late-type galaxies. The oxygen abundances are shown by filled circles, the linear least-squares fits to these data are presented by solid lines. The nitrogen abundances are shown by open squares, the linear least-squares fits to these data are presented by dashed lines. The nitrogen-to-oxygen abundance ratios are shown by open circles, the linear least-squares fits to these data are presented by solid lines. The galactocentric distances are normalized to the isophotal radius.

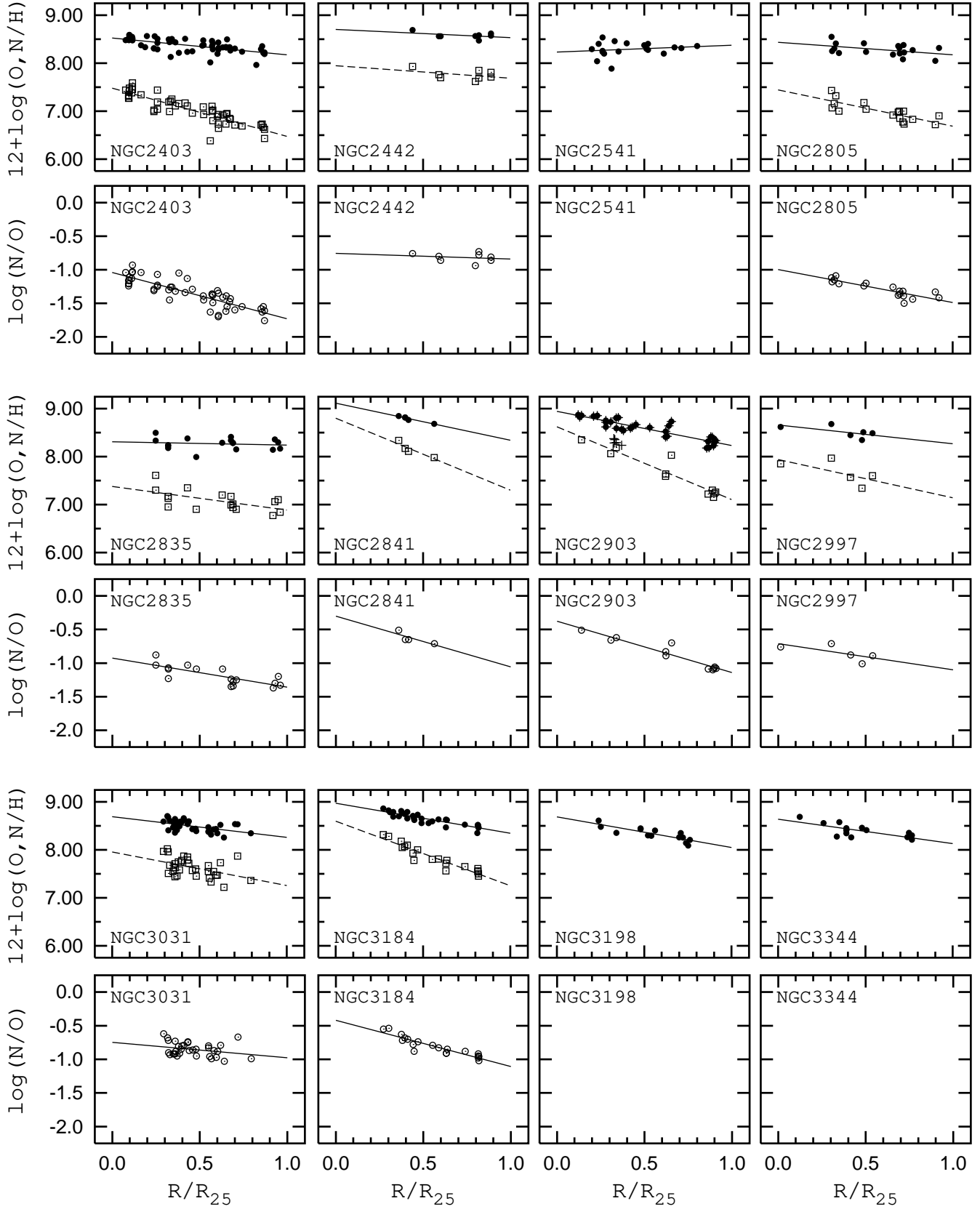


Fig. 2. Oxygen and nitrogen abundances and nitrogen-to-oxygen abundance ratio versus galactocentric distance for late-type galaxies. The oxygen abundances are shown by filled circles, the linear least-squares fits to these data are presented by solid lines. The nitrogen abundances are shown by open squares, the linear least-squares fits to these data are presented by dashed lines. The nitrogen-to-oxygen abundance ratios are shown by open circles, the linear least-squares fits to these data are presented by solid lines. The galactocentric distances are normalized to the isophotal radius. The H II regions with depleted oxygen abundances in NGC 2903 are shown by pluses.

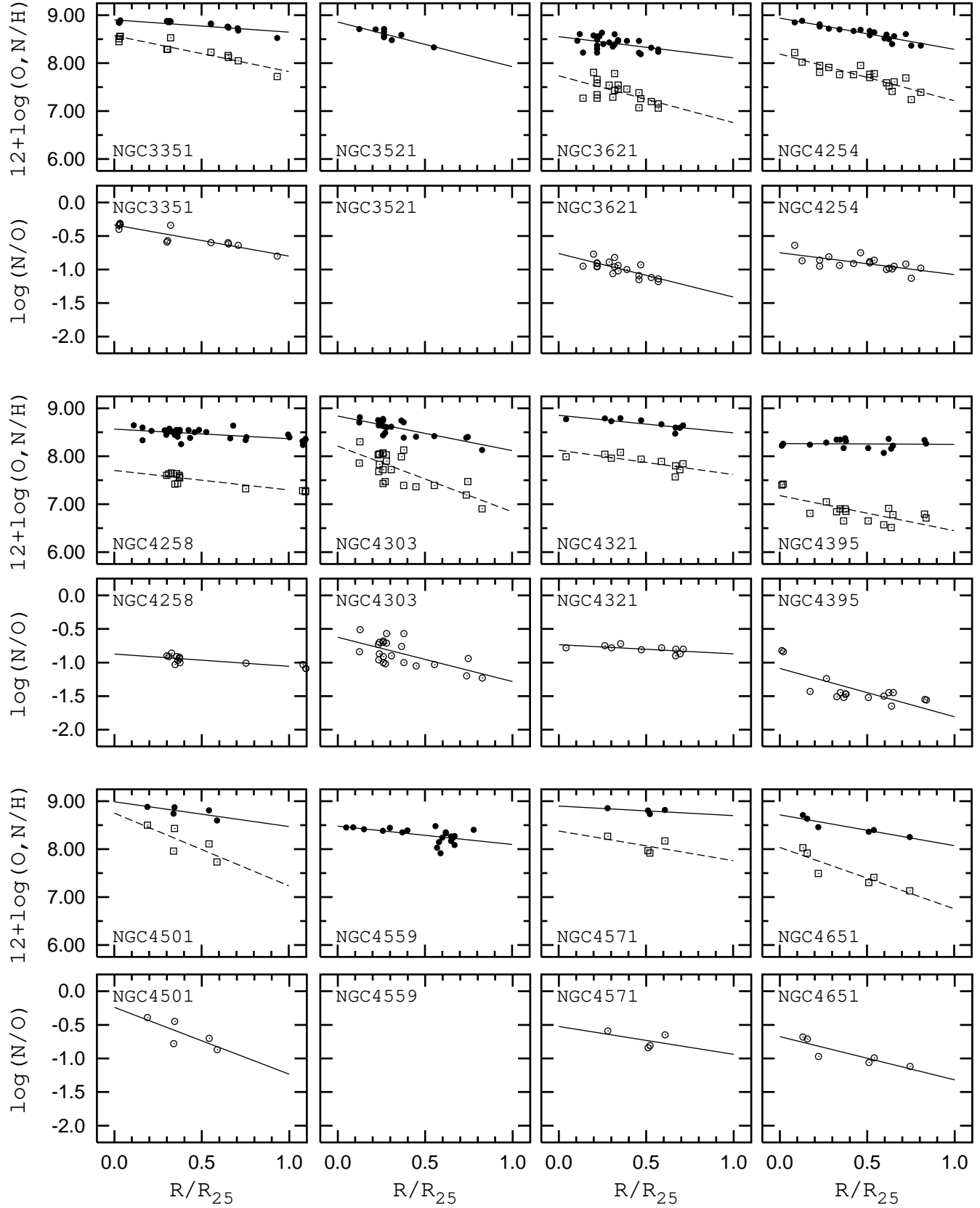


Fig. 3. Oxygen and nitrogen abundances and nitrogen-to-oxygen abundance ratio versus galactocentric distance for late-type galaxies. The oxygen abundances are shown by filled circles, the linear least-squares fits to these data are presented by solid lines. The nitrogen abundances are shown by open squares, the linear least-squares fits to these data are presented by dashed lines. The nitrogen-to-oxygen abundance ratios are shown by open circles, the linear least-squares fits to these data are presented by solid lines. The galactocentric distances are normalized to the isophotal radius.

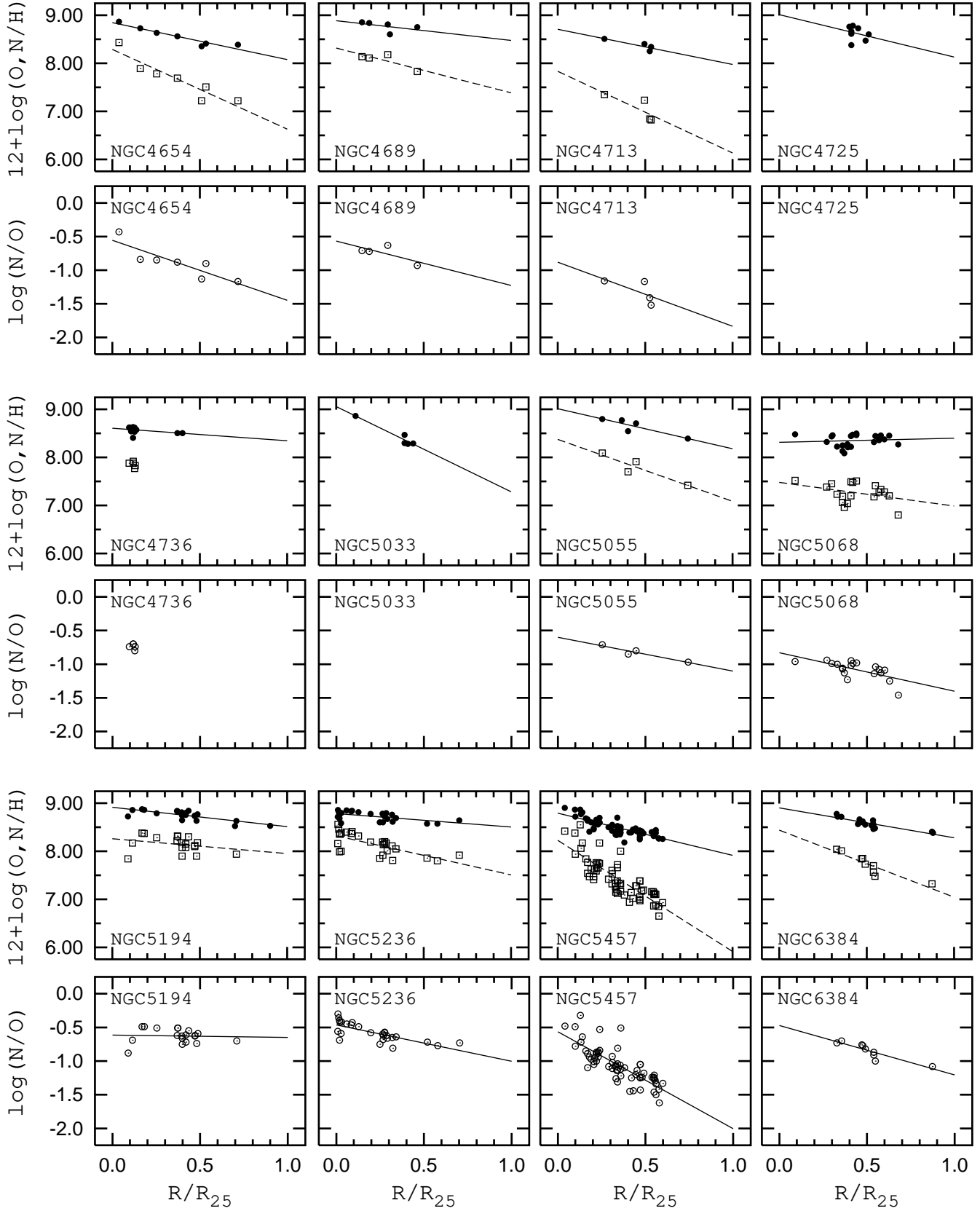


Fig. 4. Oxygen and nitrogen abundances and nitrogen-to-oxygen abundance ratio versus galactocentric distance for late-type galaxies. The oxygen abundances are shown by filled circles, the linear least-squares fits to these data are presented by solid lines. The nitrogen abundances are shown by open squares, the linear least-squares fits to these data are presented by dashed lines. The nitrogen-to-oxygen abundance ratios are shown by open circles, the linear least-squares fits to these data are presented by solid lines. The galactocentric distances are normalized to the isophotal radius.

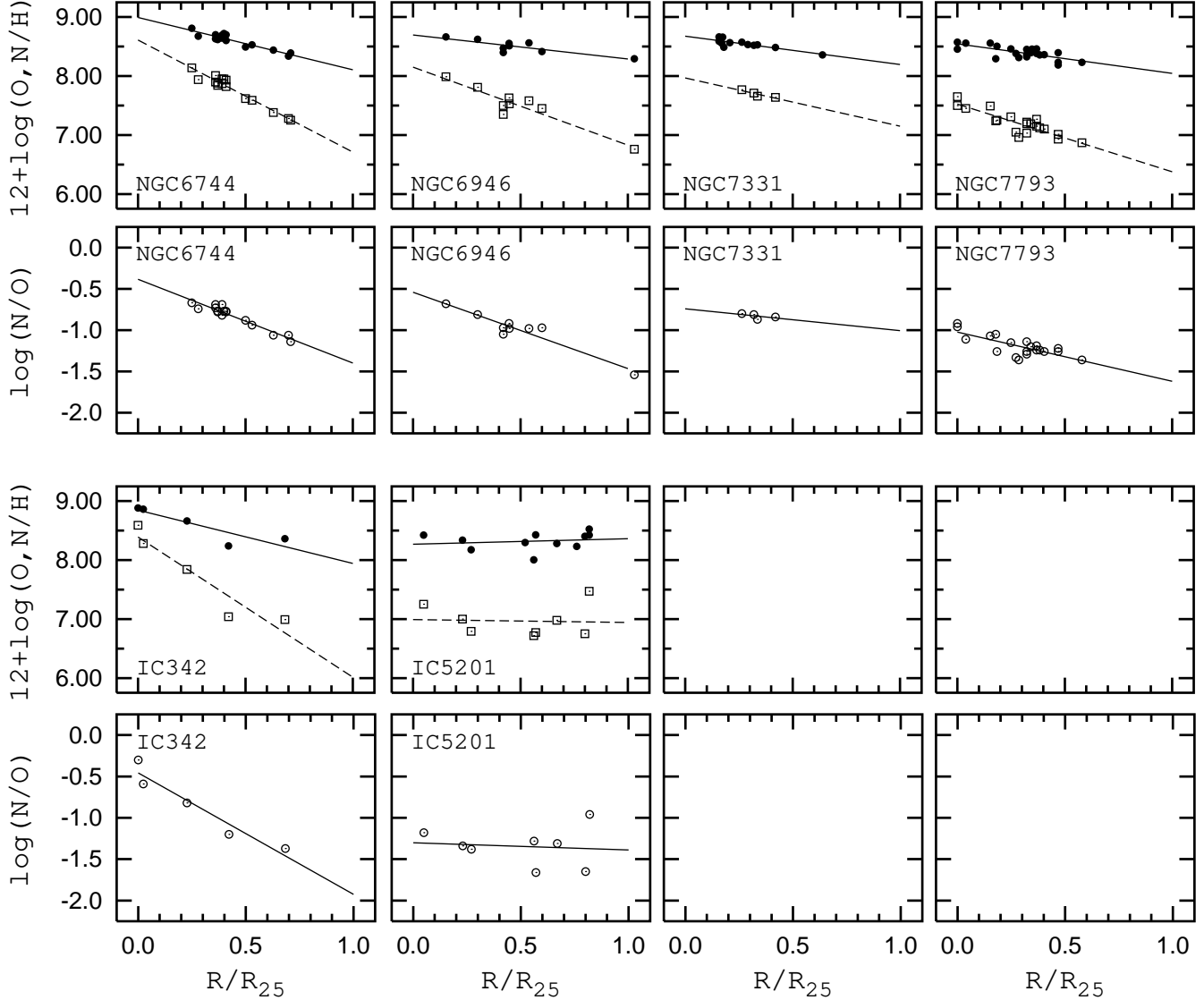


Fig. 5. Oxygen and nitrogen abundances and nitrogen-to-oxygen abundance ratio versus galactocentric distance for late-type galaxies. The oxygen abundances are shown by filled circles, the linear least-squares fits to these data are presented by solid lines. The nitrogen abundances are shown by open squares, the linear least-squares fits to these data are presented by dashed lines. The nitrogen-to-oxygen abundance ratios are shown by open circles, the linear least-squares fits to these data are presented by solid lines. The galactocentric distances are normalized to the isophotal radius.

emission line flux measurements in the H II regions is(are) reported in column 7. The list of references to Table 1 is given in Table 2.

The derived radial distributions of the oxygen abundance in galaxies are presented in Figs. 1 to 5. The oxygen abundances for individual H II regions are shown by the filled circles. The linear best fits (derived via the least squares method) to these points are presented by solid lines. The galactocentric distances are normalized to the isophotal radius.

As in the case of the oxygen abundance, the radial nitrogen abundance distribution in every galaxy is well fitted by the following equation:

$$12 + \log(N/H) = 12 + \log(N/H)_0 + C_{N/H} \times (R/R_{25}), \quad (10)$$

and the radial distribution of the nitrogen to oxygen abundance ratios is well fitted by the single equation of the type:

$$\log(N/O) = \log(N/O)_0 + C_{N/O} \times (R/R_{25}). \quad (11)$$

The derived parameters of the nitrogen abundance distributions are presented in Table 3. The name of the galaxy is listed in column 1. The extrapolated central $12 + \log(N/H)_0$ nitrogen abundance and the gradient (the coefficient $C_{N/H}$ in Eq.(10)) expressed in terms of dex/ R_{25} are listed in columns 2 and 3. The scatter of nitrogen abundances around the general radial nitrogen abundance trend is reported in column 4. The number of available individual spectra of H II regions in the galaxy with measured nitrogen emission line fluxes is listed in column 5.

Table 3. The derived parameters of the radial distributions of the nitrogen abundance and nitrogen-to-oxygen abundance ratios for our sample of galaxies

galaxy	$12+\log(\text{N}/\text{H})_0$	gradient dex/ R_{25}	$\Delta\log(\text{N}/\text{H})$ dex	number of H II regions	$\log(\text{N}/\text{O})_0$	gradient dex/ R_{25}	$\Delta\log(\text{N}/\text{O})$
NGC0224	8.17	-1.24	0.15	22	-0.59	-0.71	0.09
NGC0253	7.81	-0.79	0.17	9	-0.90	-0.26	0.09
NGC0300	7.29	-0.72	0.19	15	-1.17	-0.37	0.12
NGC0598	7.48	-0.74	0.11	29	-1.08	-0.53	0.10
NGC0628	7.92	-0.95	0.13	36	-0.77	-0.51	0.09
NGC0753	8.14	-0.48	0.18	11	-0.66	-0.30	0.14
NGC0925	7.50	-1.27	0.10	17	-1.00	-0.74	0.04
NGC1058	7.89	-0.68	0.12	6	-0.81	-0.36	0.08
NGC1068							
NGC1232	8.09	-1.22	0.12	15	-0.64	-0.64	0.06
NGC1365	8.05	-1.20	0.19	53	-0.69	-0.50	0.08
NGC1637	8.04	-0.18	0.21	14	-0.63	-0.18	0.12
NGC2403	7.48	-1.01	0.14	50	-1.04	-0.69	0.11
NGC2442	7.95	-0.26	0.08	8	-0.75	-0.09	0.06
NGC2541							
NGC2805	7.44	-0.75	0.12	17	-1.00	-0.49	0.06
NGC2835	7.38	-0.50	0.16	17	-0.93	-0.43	0.09
NGC2841	8.80	-1.50	0.05	4	-0.30	-0.75	0.04
NGC2903	8.62	-1.52	0.14	11	-0.38	-0.76	0.06
NGC2997	7.94	-0.80	0.17	5	-0.71	-0.39	0.08
NGC3031	7.96	-0.70	0.17	33	-0.75	-0.23	0.10
NGC3184	8.60	-1.35	0.08	20	-0.42	-0.69	0.05
NGC3198							
NGC3344							
NGC3351	8.57	-0.75	0.08	13	-0.33	-0.47	0.06
NGC3521							
NGC3621	7.74	-0.98	0.17	19	-0.76	-0.65	0.07
NGC4254	8.19	-0.97	0.11	18	-0.75	-0.33	0.08
NGC4258	7.70	-0.41	0.07	13	-0.87	-0.18	0.04
NGC4303	8.21	-1.37	0.23	22	-0.62	-0.66	0.15
NGC4321	8.12	-0.51	0.10	10	-0.73	-0.14	0.04
NGC4395	7.18	-0.73	0.17	16	-1.09	-0.72	0.15
NGC4501	8.75	-1.52	0.18	5	-0.24	-1.00	0.12
NGC4559							
NGC4571	8.38	-0.62	0.12	4	-0.52	-0.41	0.09
NGC4651	8.04	-1.28	0.14	6	-0.67	-0.64	0.08
NGC4654	8.29	-1.66	0.14	7	-0.56	-0.89	0.11
NGC4689	8.32	-0.93	0.08	4	-0.57	-0.66	0.08
NGC4713	7.84	-1.70	0.14	4	-0.88	-0.95	0.12
NGC4725							
NGC4736							
NGC5033							
NGC5055	8.38	-1.29	0.10	4	-0.60	-0.50	0.03
NGC5068	7.48	-0.49	0.18	19	-0.03	-0.57	0.10
NGC5194	8.26	-0.31	0.15	19	-0.61	-0.04	0.10
NGC5236	8.32	-0.82	0.15	27	-0.46	-0.54	0.09
NGC5457	8.23	-2.32	0.22	63	-0.56	-1.44	0.16
NGC6384	8.44	-1.40	0.10	9	-0.47	-0.73	0.05
NGC6744	8.61	-1.90	0.06	16	-0.38	-1.01	0.04
NGC6946	8.15	-1.32	0.11	9	-0.54	-0.92	0.07
NGC7331	7.97	-0.82	0.02	4	-0.74	-0.27	0.02
NGC7793	7.53	-1.15	0.10	20	-1.02	-0.60	0.08
IC0342	8.39	-2.38	0.21	5	-0.46	-1.46	0.11
IC5201	6.99	-0.05	0.25	8	-1.30	-0.09	0.22

Table 4. Galaxies with the observed H II regions which are expected to not belong to the upper branch of the $R_{23} - O/H$ diagram and the radius R^* where the oxygen abundance decreases to around $12+\log(O/H) = 8.2$.

galaxy	R^*/R_{25}	galaxy	R^*/R_{25}
NGC300	0.8	NGC4651	0.8
NGC925	0.5	NGC5033	0.5
NGC1365	0.7	NGC5457	0.6
NGC2805	0.9	NGC7793	0.6
NGC3198	0.8	IC342	0.7

The extrapolated central value of the nitrogen-to-oxygen ratio $\log(N/O)_0$ is listed in column 6. The radial gradient of the nitrogen-to-oxygen abundance ratio (the coefficient $C_{N/O}$ in Eq.(11)) expressed in terms of dex/R_{25} is reported in column 7. The scatter of $\log(N/O)$ values around the general radial trend is presented in column 8. The nitrogen emission line fluxes in the H II regions were taken from the same sources as the oxygen emission line fluxes (see references in Table 1).

The derived radial distributions of the nitrogen abundances and nitrogen-to-oxygen abundance ratios in galaxies are shown in Figs.1 to 5. The nitrogen abundances for individual H II regions are shown by the open squares. The linear best fits to these points are presented by dashed lines. The nitrogen-to-oxygen abundance ratios for individual H II regions are shown by the open circles. The linear best fits to these points are presented by solid lines.

For the majority of galaxies, all the H II regions with available oxygen and nitrogen emission line measurements were used in the analysis of the abundance gradients. For a few galaxies, however, some H II regions were rejected for the following reason. The relationship between oxygen abundance and strong line intensities is double-valued with two distinct parts usually known as the “lower” and “upper” branches of the $R_{23} - O/H$ relationship. Thus, one has to know apriori on which of the two branches the H II region lies. The above expression for the oxygen abundance determination in H II regions, Eq.(1), is valid only for H II regions which belong to the upper branch, with $12+\log(O/H)$ higher than ~ 8.2 . It has been known for a long time (Searle 1971; Smith 1975) that disks of spiral galaxies show radial oxygen abundance gradients, in the sense that the oxygen abundance is higher in the central part of the disk and decreases with galactocentric distance. We thus start from the H II regions in the central part of disks and move outward until the radius R^* where the oxygen abundance decreases to $12+\log(O/H) \sim 8.2$. It should be noted that it is difficult to establish the exact value of R^* due to the scatter in oxygen abundance values at any fixed radius. An unjustified use of Eq. (1) in the determination of the oxygen abundance in low-metallicity H II regions beyond R^* would result in overestimated oxygen abundances, and would produce a false bend in the slope of abundance gradients (Pilyugin 2003a). Therefore,

H II regions with galactocentric distances larger than R^* , those with $12+\log(O/H)$ less than 8.2 were rejected. The list of such galaxies is given in Table 4.

The credibility of the radial oxygen abundance gradients (as well as gradients of the nitrogen abundance and gradients of the nitrogen-to-oxygen abundance ratios) is defined not only by the large number of H II regions and their small dispersion but also by the distribution of these H II regions along the galactic radius. For example, the six H II regions in the galaxy NGC 4651 (Fig. 3) give a much more reliable value of abundance gradients than the 8 H II regions in the galaxy NGC 4725 (Fig. 4). The estimated values of the radial oxygen abundance gradient in galaxies NGC 1068, NGC 1637, NGC 2841, NGC 3521, NGC 4571, NGC 4713, NGC 4725, NGC 5033, and NGC 5055 are not beyond question.

3. Characteristic oxygen abundance in spirals as a function of M_B , V_{rot} , and Hubble type

As was noted above, in investigations of the relationships between the oxygen abundances and the macroscopic properties of spiral galaxies, the concept of the characteristic oxygen abundance has been introduced: it is defined as the oxygen abundance in the disk at a predetermined galactocentric distance. Following Zaritsky, Kennicutt & Huchra (1994), the value of the oxygen abundance at $r = 0.4R_{25}$ will be used here as the *characteristic* oxygen abundance in a galaxy. To derive a reliable galaxy luminosity the accurate value of the distance is necessary. The compilation of the up-to-date distance measurements for our sample of galaxies is discussed in the Appendix.

The characteristic oxygen abundance in spiral galaxies as a function of absolute blue magnitude M_B is shown in Fig. 6. The solid line is the characteristic oxygen abundance – luminosity relationship (linear best fit derived through the least squares method):

$$12 + \log(O/H) = 6.93 (\pm 0.37) - 0.079 (\pm 0.018) M_B. \quad (12)$$

The dashed lines correspond to this relation shifted by -0.2 dex and $+0.2$ dex. Fig. 6 clearly demonstrates that there is a correlation between the characteristic oxygen abundance of a galaxy and its blue luminosity. The bulk of the galaxies lies within the band defined by the dashed lines (± 0.2 dex around the best fit). The dotted line in Fig. 6 is the luminosity – metallicity relationship for irregular galaxies (see below) extrapolated to the luminosity range of spiral galaxies. The line presented in Fig. 6 by the plus signs is the extrapolated $O/H - M_B$ relationship for irregular galaxies derived by Richer & McCall (1995). Inspection of Fig. 6 shows that the slope of the derived luminosity – metallicity relationship for spiral galaxies is lower than the one for irregular galaxies.

We have carried out a search in the literature for measurements of rotation velocities for our sample of spiral galaxies. Unfortunately, a measurement of the rotation velocity is not available for 7 galaxies of our sample. On the

Table 5. The characteristic oxygen abundance (at $r = 0.4R_{25}$), gas (atomic and molecular) mass fraction μ , atomic and molecular hydrogen contents, and rotation velocity for spiral galaxies from our sample. The oxygen abundance is given as $12+\log(\text{O}/\text{H})$.

galaxy	O/H	μ	M_{H_1}/L_B	M_{H_2}/L_B	V_{rot}	references
NGC			M_\odot/L_\odot	M_\odot/L_\odot	km/s	$(M_{H_1}; M_{H_2}; V_{rot})$
224	8.55	0.09	0.15	0.004	269	DD, HR ; KDI ; H
253	8.50	0.12	0.15	0.057	215	SD, HR, HS ; YXT, SNK ; PCG, H
300	8.33	0.38	0.93	95	RCC, HR ; - ; PCB, H, RCC
598	8.49	0.24	0.46	0.004	116	DD, HR ; YXT ; H, CS
628	8.51	0.35	0.76	0.052	153	WKA, R, SD, DD ; NN, YXT, S, HTR ; NNK
753	8.73	0.18	0.33	215	Sh, BSC ; - ; RFT, AMB
925	8.32	0.28	0.58	0.013	127	WKA, R, DD, HHG ; S ; KS
1058	8.58	0.35	0.79	0.017	SD, vKS ; S ; -
1068	8.73	0.10	0.04	0.117	220	HS, HBS ; YXT ; HB
1232	8.50	0.19	0.35	229	SD, RMG, ZB, BMR ; - ; ZB, BMR
1365	8.46	0.21	0.27	0.130	285	OH, RMG, JM ; SJL ; OH
2403	8.39	0.31	0.67	0.004	135	WKA, R, HR ; YXT, S ; H, BBS
2442	8.64	0.11	0.18	0.013	BM, RMG, RKS ; BWR ; -
2541	8.29	0.43	1.16	R, BR, HS, HHM ; - ; -
2805	8.33	0.29	0.63	78	Sh, Re, BCH ; - ; Re
2835	8.28	0.19	0.35	120	SD, RMG, BMR ; - ; BMR
2841	8.81	0.16	0.23	0.052	318	R, B, HS ; YXT ; BBS, B
2903	8.66	0.15	0.22	0.043	223	WKA, HR, HS, HHG, HHM ; NN, YXT, S, HTR ; NNK, BBS
2997	8.51	0.13	0.22	195	SD, RMG ; - ; P, MM
3031	8.52	0.10	0.16	0.004	240	ADS, HR ; S ; H, Ro
3184	8.72	0.21	0.34	0.052	Sh, HS ; NN, YXT, S ; -
3198	8.43	0.28	0.57	154	WKA, R, SD ; - ; ABB, HRG, BBS
3344	8.43	0.29	0.60	0.030	R, HHG ; YXT, S ; -
3351	8.80	0.10	0.14	0.035	236	Sc, HS ; YXT, S, HTR ; Bu
3521	8.49	0.22	0.33	0.091	235	R ; NN, YXT, S, HTR ; NNK, CG
3621	8.38	0.34	0.78	163	RMG, HR, BMR ; - ; BMR
4254	8.68	0.18	0.20	0.126	264	SD, Wb, HRb ; YXT, SKB, SEC, KY ; NNK, GGK, Wb
4258	8.49	0.14	0.23	0.022	200	WKA, R, HS ; YXT, HTR, CD ; AS
4303	8.55	0.17	0.20	0.104	178	Sh, Wb, HS, HRb ; YXT, SKB, HTR, KY ; NNK, GGK, Wb
4321	8.71	0.15	0.12	0.139	236	Sh, Wa, HRb ; YXT, SKB, HTR, KY ; GGK, Wa
4395	8.26	0.43	1.07	0.083	83	WKA, R, HR, HS, HHM ; SEC ; BB
4501	8.78	0.09	0.07	0.083	295	Wa, HRb ; YXT, SKB, KY ; NNK, GGK, Wa, KS
4559	8.33	0.27	0.54	0.017	129	BR, Sh, HS ; S ; KS
4571	8.82	0.12	0.14	0.078	165	Wb, HR, HRb ; YXT, KY ; Wb
4651	8.46	0.19	0.33	0.035	250	Wa, HHG, HRb ; YXT, SKB, KY ; Wa
4654	8.54	0.15	0.20	0.070	195	Sh, Wb, HRb ; YXT, SKB, KY ; GGK, Wb
4689	8.72	0.10	0.05	0.104	182	Wb, HRb ; YXT, SKB, SEC, KY ; GGK, Wb
4713	8.42	0.29	0.58	0.017	137	Sh, Wb, HRb, HHM ; YXT, KY ; Wb
4725	8.66	0.14	0.18	0.065	249	WKA, GDH, WAD ; YXT - ; Bu, WAD
4736	8.50	0.05	0.05	0.022	198	R, BHS, HR ; NN, YXT, S, HTR ; NNK, Bu, BHS
5033	8.35	0.28	0.50	0.096	228	WKA, R, SD, B ; YXT, SEC, HTR ; NNK, HAS, B
5055	8.68	0.24	0.42	0.061	210	WKA, R, B ; YXT, S, HTR ; TM, B
5068	8.35	0.18	0.34	RMG, HR ; - ; -
5194	8.75	0.14	0.14	0.109	242	WG, DD ; YXT, S, HTR ; KN, WG
5236	8.68	0.31	0.57	0.104	205	SD, HR, DD ; YXT ; VPD
5457	8.44	0.32	0.69	0.026	180	R, DD, HR ; S, HTR ; GW
6384	8.65	0.19	0.29	0.070	200	Sh, HHM ; YXT ; SCR
6744	8.64	0.31	0.67	RMG ; - ; -
6946	8.53	0.15	0.22	0.048	179	R, DD, HR ; YXT, S, HTR ; NNK, H, CCB
7331	8.48	0.18	0.24	0.078	262	R, Sh, B ; NN, YXT, HTR, HHM ; NNK, BBS, B, KS
7793	8.34	0.18	0.31	0.013	117	CP, RMG, HR, BMR ; SEC ; CP, BMR
IC0342	8.49	0.16	0.26	0.026	192	R, HR ; YXT, S ; H
IC5201	8.31	0.36	0.86	97	BM, RMG, BMR ; - ; BMR

Table 6. List of references to Table 5

Abbr	Reference	Abbr	Reference
ABB	van Albada, Bahcall, Begeman, et al. 1985	KN	Kuno & Nakai 1997
ADS	Appleton, Davies & Stephenson 1981	KS	Krumm & Salpeter 1979
AMB	Amram, Marcelin, Balkowski, et al. 1994	KY	Kenney & Young 1988
AS	van Albada & Shane 1975	MM	Milliard & Marcelin 1981
B	Bosma 1981	NN	Nishiyama & Nakai 2001
Bu	Buta 1988	NNK	Nishiyama, Nakai & Kuno 2001
BB	de Blok & Bosma 2002	OH	Ondrechen & van der Hulst 1989
BBS	Begeman, Broeils & Sanders 1991	P	Peterson 1978
BCH	Bosma, Casini, Heidmann, et al. 1980	PCB	Puche, Carignan & Bosma 1990
BHS	Bosma, van der Hulst & Sullivan 1977	PCG	Puche, Carignan & van Gorkom 1991
BM	Bajaja & Martin 1985	R	Rots 1980
BMR	Becker, Mebold, Reif, et al. 1988	RCC	Rogstad, Crutcher & Chu 1979
BR	Broeils & Rhee 1997	Re	Reakes 1979
BSC	Bravo-Alfaro, Szomoru, Cayatte, et al. 1997	Ro	Rots 1975
BWR	Bajaja, Wielebinski, Reuter, et al. 1995	RFT	Rubin, Ford & Thonnard 1980
CCB	Carignan, Charbonneau, Boulanger, et al. 1990	RKS	Ryder, Koribalski, Staveley-Smith, et al. 2001
CD	Cox & Downes 1996	RMG	Reif, Mebold, Goss, et al. 1982
CG	Casertano & van Gorkom 1991	S	Sage 1993
CS	Corbelli & Salucci 2000	Sc	Schneider 1989
DD	Dean & Davies 1975	SCR	Sperandio, Chincarini, Rampazzo, et al. 1995
GDH	García-Barreto, Downes & Huchtmeier 1994	Sh	Shostak 1978
GGK	Guhathakurta, vanGorkom, Kotanyi, et al. 1988	SD	Staveley-Smith & Davies 1988
GW	Guélin & Weliachew 1970	SEC	Stark, Elmegreen & Chance 1987
H	Huchtmeier 1975	SJL	Sandqvist, Jörsäter & Lindblad 1995
HAS	Hoekstra, van Albada & Sancisi 2001	SKB	Stark, Knapp, Bally, et al 1986
HB	Helfer & Blitz 1995	SNK	Sorai, Nakai, Kuno, et al 2000
HBS	Heckman, Balick & Sullivan 1978	TM	Thornley & Mundy 1997
HHG	Hewitt, Haynes & Giovanelli 1983	vKS	van der Kruit & Shostak 1984
HHM	Haynes, Hogg, Maddalena, et al. 1998	VPD	de Vaucouleurs, Pence & Davoust 1983
HR	Huchtmeier & Richter 1986a	Wa	Warmels 1988a
HRb	Huchtmeier & Richter 1986b	Wb	Warmels 1988b
HRG	Hunter, Rubin & Gallagher 1986	WAD	Wevers, Appleton, Davies, et al. 1984
HS	Huchtmeier & Seiradakis 1985	WG	Weliachew & Gottesman 1973
HTR	Helfer, Thornley, Regan, et al. 2003	WKA	Wevers, van der Kruit & Allen 1986
JM	Jörsäter & van Moorsel 1995	YXT	Young, Xie & Tacconi 1995
KDI	Koper, Dame, Israel, et al. 1991	ZB	van Zee & Bryant 1999

contrary, there are two or more measurements of rotation velocities for a number of galaxies. The more recent value (or a mean value if the measurements are close to each other) is taken for these galaxies. The adopted values of the rotation velocity for the galaxies and corresponding reference(s) are listed in Table 5 and Table 6.

The characteristic oxygen abundance in spiral galaxies as a function of rotation velocity V_{rot} is shown in Fig. 7. The solid line is the oxygen abundance – rotation velocity relationship (linear best fit)

$$12 + \log(O/H) = 8.18 (\pm 0.06) + 0.00179 (\pm 0.00031) V_{\text{rot}}. \quad (13)$$

The dotted lines correspond to this relation shifted by -0.2 dex and $+0.2$ dex. Fig. 7 shows that the characteristic oxygen abundance of a galaxy correlates with its rotation velocity. The deviation of an individual galaxy from the general trend is usually less than 0.2 dex. The mean value of the scatter in the characteristic oxygen abundances at a given rotation velocity is 0.12 dex for 46 points.

The characteristic oxygen abundance in spiral galaxies as a function of morphological type, expressed in terms of T -type, is shown in Fig. 8. The solid line is the characteristic oxygen abundance – T relationship (best fit)

$$12 + \log(O/H) = 8.81 (\pm 0.06) - 0.059 (\pm 0.011) T. \quad (14)$$

The dotted lines correspond to this relation shifted by -0.2 dex and $+0.2$ dex. Fig. 8 shows that the characteristic oxygen abundance of a galaxy correlates with its morphological type. The deviation of an individual galaxy from the general trend usually does not exceed the value ± 0.2 dex, as in the cases of the $O/H - M_B$ and the $O/H - V_{\text{rot}}$ diagrams. The mean value of the scatter in the characteristic oxygen abundances at a given morphological type is 0.13 dex for 53 points.

One can see that the characteristic oxygen abundance correlates well with both the absolute blue luminosity, the rotational velocity, and the morphological type; the correlation with the rotation velocity perhaps being slightly tighter.

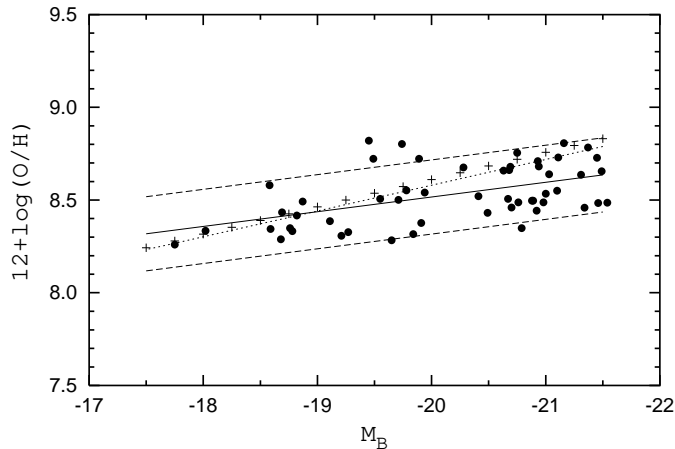


Fig. 6. The characteristic oxygen abundance as a function of absolute blue magnitude M_B for our sample of spiral galaxies. The solid line is the $O/H - M_B$ relationship (best fit derived through the least squares method). The dashed lines correspond to the lines shifted by -0.2 dex and $+0.2$ dex along the vertical axes relatively to the derived $O/H - M_B$ relationship. The dotted line is the $O/H - M_B$ relationship for our sample of irregular galaxies extrapolated to the luminosity range of spiral galaxies. The line presented by the plus signs is the extrapolated $O/H - M_B$ relationship for irregular galaxies derived by Richer & McCall (1995).

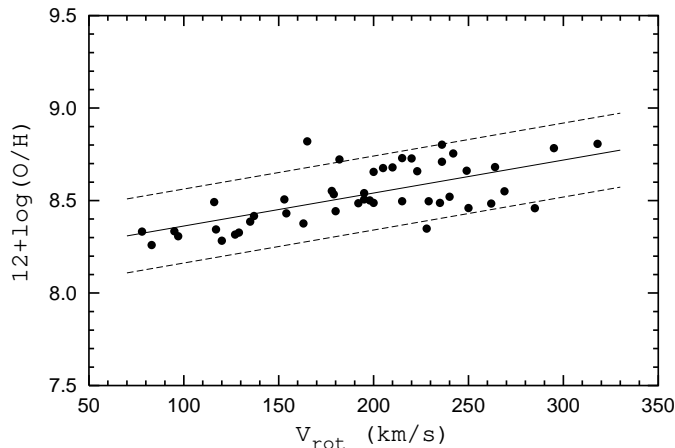


Fig. 7. The characteristic oxygen abundance as a function of rotation velocity for our sample of spiral galaxies. The solid line is the $O/H - V_{\text{rot}}$ relationship (best fit derived through the least squares method). The dashed lines correspond to the lines shifted by -0.2 dex and $+0.2$ dex relatively to the derived $O/H - V_{\text{rot}}$ relationship.

4. Comparison between $O/H - M_B$ relationship for spiral and irregular galaxies

Zaritsky, Kennicutt & Huchra (1994) found that the characteristic gas-phase oxygen abundance – luminosity relation of spiral galaxies extends almost directly to the luminosity – metallicity relationship of irregular galaxies. Melbourne & Salzer (2002) and Lamareille et al. (2004)

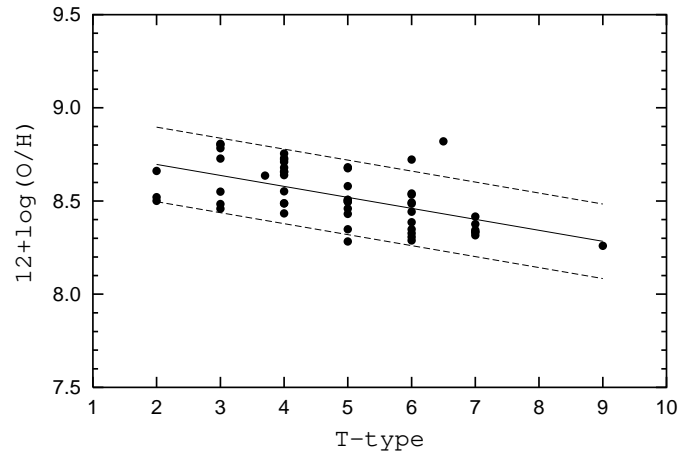


Fig. 8. The characteristic oxygen abundance as a function of Hubble type, expressed in the terms of T-type, for our sample of spiral galaxies. The solid line is the $O/H - T$ relationship derived through the least squares method. The dashed lines correspond to the lines shifted by -0.2 dex and $+0.2$ dex relatively to the derived $O/H - T$ relationship.

found that the slope of the oxygen abundance – luminosity relationship for high-luminosity galaxies is steeper than when dwarf galaxies are considered alone and may be evidence that the relationship is not linear over the full luminosity range. Garnett (2002) concluded that the metallicity – luminosity correlation shows a roughly uniform growth in the average present-day O/H abundance over 11 mag in absolute blue magnitude M_B . Let us compare the derived metallicity – luminosity relationship for spiral galaxies with that for irregular galaxies.

The irregular galaxies were selected from the samples of Richer & McCall (1995) and Pilyugin (2001c). The luminosities and oxygen abundances for irregular galaxies are taken from these studies and are listed in Cols. 3 and 4 of Table 7. The values of the gas mass fraction in the irregular galaxies were estimated taking into account the atomic hydrogen mass only since the molecular hydrogen in dwarf irregular galaxies is only a small fraction of the total gas mass. The HI fluxes were taken mainly from Karachentsev, Makarov & Huchtmeier (1999). The derived values of gas mass fraction μ in irregular galaxies are reported in Col. 5 of Table 7. The rotation velocities for irregular galaxies taken from the literature, the values of the rotation velocity and corresponding references to the sources are listed in Cols. 6 and 7 of Table 7.

The oxygen abundances in spiral and irregular galaxies are plotted versus absolute blue magnitude M_B in Fig. 9. The filled circles in Fig. 9 are spiral galaxies, and the solid line is the $O/H - M_B$ relationship for spiral galaxies, Eq. (12). The open squares in Fig. 9 are irregular galaxies from Table 7. The dashed line is the $O/H - M_B$ relationship (best fit) for irregular galaxies

$$12 + \log(O/H) = 5.80 (\pm 0.17) - 0.139 (\pm 0.011) M_B \quad (15)$$

Table 7. Data for irregular galaxies. *References* – (a) Lee, McCall, Kingsburgh, et al. 2003; (b) Pilyugin 2001c; (c) Karachentsev, Makarov & Huchtmeier 1999; (d) Skillman, Terlevich, Teuben & van Woerden 1988; (e) Hoffman, Salpeter, Farhat, et al. 1996; (f) Côté, Carignan & Freeman 2000; (g) Kinman & Davidson 1981; (h) Richer & McCall 1995; (i) Wilcots & Miller 1998; (j) Alves & Nelson 2000.

galaxy	T-type	M_B	$12+\log O/H$	μ	V_{rot} km/s	references (M_B , O/H, μ , V_{rot})
Sextans B	10	-14.02	7.86	0.43	24	a, b, c, c
Sextans A	10	-14.04	7.71	0.60	37	a, b, c, d
GR 8	10	-12.19	7.60	0.54	13	a, b, c, e
WLM	10	-13.92	7.78	0.44	31	a, b, c, c
UGC 4483	10	-12.80	7.47	0.68	22	b, b, c, c
UGC 5423	10	-12.90	7.81	0.36	27	b, b, c, c
UGC 6456	10	-13.24	7.71	0.68	24	b, b, c, c
Leo A	10	-11.53	7.27	0.58	16	a, b, c, c
UGCA 292	10	-11.43	7.22	0.83	12	b, b, c, c
DDO 167	10	-13.30	7.81	0.50	17	b, b, c, c
SagDIG	10	-12.10	7.48	0.51	19	b, b, c, f
A1116+51	10	-14.99	7.76	0.69	–	b, b, g, –
A1228+12	10	-14.57	7.79	0.46	–	b, b, g, –
A2228-00	10	-14.57	7.79	0.65	–	b, b, g, –
ESO 245-G05	10	-15.50	7.94	0.66	48	b, b, c, i
DDO 53	10	-13.35	7.75	0.75	–	b, b, c, –
DDO 190	10	-15.10	7.74	0.51	–	b, b, c, –
Holmberg II	10	-15.98	7.92	0.57	34	a, h, c, c
IC 10	10	-15.82	8.22	0.22	30	a, h, c, i
IC 1613	10	-14.53	7.71	0.46	21	a, h, c, e
IC 2574	9	-16.85	8.08	0.50	50	h, h, c, c
IC 4662	10	-15.64	8.09	0.30	48	h, h, c, c
LMC	9	-17.73	8.35	0.20	72	h, h, c, j
NGC1560	7	-16.17	8.02	0.27	59	h, h, c, c
NGC 2366	10	-16.28	7.92	0.48	44	a, h, c, c
NGC 3109	9	-15.30	8.06	0.47	49	a, h, c, c
NGC 4214	10	-17.82	8.23	0.37	–	h, h, c, –
NGC 5408	10	-15.60	8.01	0.35	38	h, h, c, c
NGC 55	9	-18.07	8.34	0.20	71	h, h, c, c
SMC	9	-16.35	8.03	0.49	21	h, h, c, c

The dotted line is the O/H – M_B relationship for irregular galaxies

$$12 + \log(O/H) = 5.59 (\pm 0.54) - 0.153 (\pm 0.025) M_B \quad (16)$$

derived by Lee et al. (2003). The O/H – M_B relationship for irregular galaxies

$$12 + \log(O/H) = 5.67 (\pm 0.48) - 0.147 (\pm 0.029) M_B \quad (17)$$

derived by Richer & McCall (1995) is presented by the plus signs. Inspection of Fig. 9 (as well as the comparison between Eq. (15), Eq. (16), and Eq. (17)) shows that the O/H – M_B relationship for our sample of irregular galaxies agrees, within the uncertainties, with that from Lee et al. (2003) and from Richer & McCall (1995). Fig. 9 shows a familiar oxygen abundance – luminosity correlation for late-type galaxies, an increase in metallicity with luminosity over the full range of absolute blue magnitude, M_B

from ~ -22 to ~ -11 . Comparison between Eq. (12) and Eq. (15) shows that the O/H – M_B relationships for spiral and irregular galaxies have slightly different slopes.

Fig. 10 shows the oxygen abundance in spiral (filled circles) and irregular (open squares) galaxies as a function of rotation velocity V_{rot} . The most prominent feature is the bend in the O/H – V_{rot} relation. Garnett (2002) also found that the correlation between O/H and V_{rot} does not increase steadily but rather turns over for rotation speeds greater than 125 km s^{-1} . It is worth noting that the presence of the bend in the O/H – V_{rot} relation does not necessarily imply the existence of a bend in the O/H – M_B trend. Fig. 11 shows the absolute blue magnitude M_B as a function of the rotation velocity V_{rot} for spiral (filled circles) and irregular (open squares) galaxies. Inspection of Fig. 11 shows that the correlation between M_B and V_{rot} is not linear but rather shows a bend. This bend in the

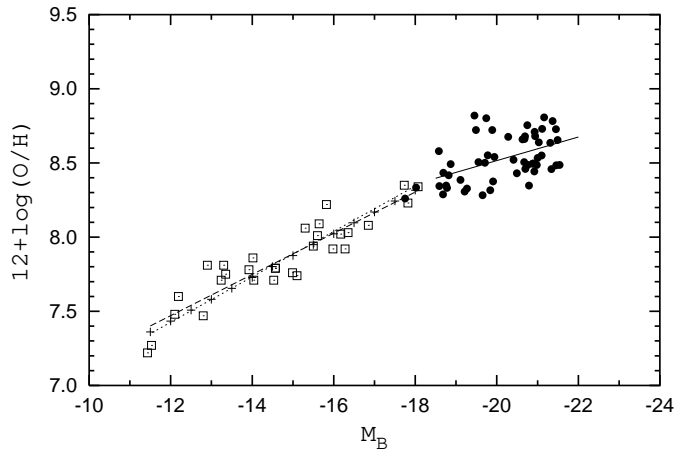


Fig. 9. The characteristic oxygen abundance as a function of absolute blue magnitude M_B for our sample of spiral galaxies (the filled circles). The solid line is the best (linear least-squares) fit to these data. The open squares are oxygen abundances in irregular galaxies, the dashed line is the metallicity – luminosity relationship for our sample of irregular galaxies. The dotted line is the $O/H - M_B$ relationship for irregular galaxies derived by Lee et al. (2003). The $O/H - M_B$ relationship for irregular galaxies derived by Richer & McCall (1995) is presented by the plus signs.

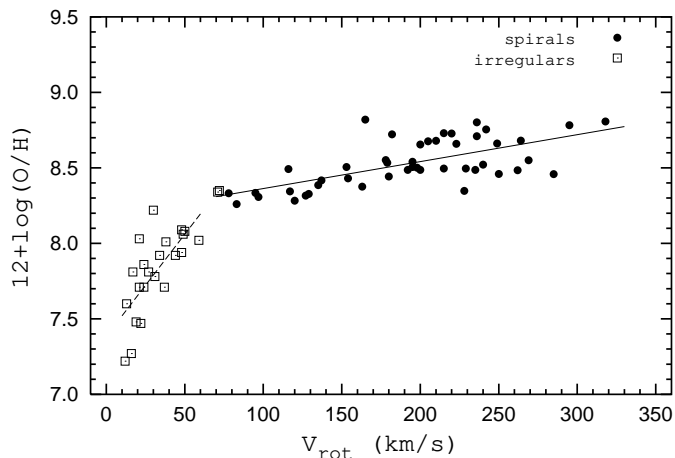


Fig. 10. The characteristic oxygen abundance as a function of rotation velocity V_{rot} for our sample of spiral galaxies (the filled circles). The solid line is the best (linear least-squares) fit to these data. The open squares are oxygen abundances in irregular galaxies, the dashed line is the linear least-squares fit to these data.

$O/H - V_{rot}$ trend would thus occur even if the increase in oxygen abundance with luminosity can be described by a single linear function over the full magnitude range.

5. The effective oxygen yields

The observed oxygen abundance in a galaxy is defined not only by the astration level but also by the mass exchange between a galaxy and its environment. The latter can alter the relation between oxygen abundance and gas mass

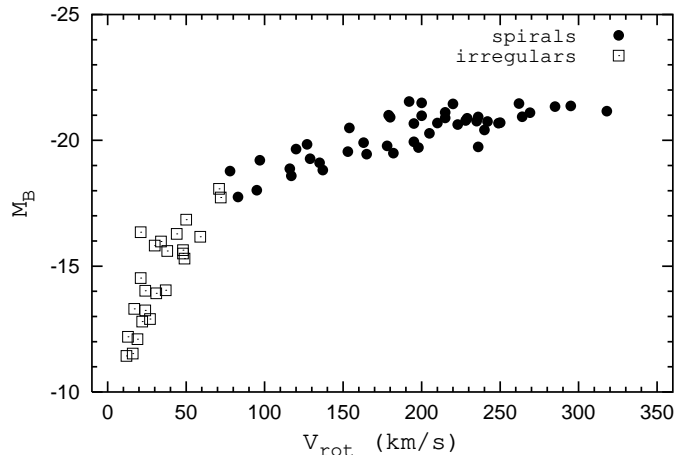


Fig. 11. The absolute blue magnitude M_B as a function of the rotation velocity. The filled circles are spiral galaxies, the open squares are irregular galaxies.

fraction; it mimics the variation in the oxygen yield. To investigate the possibility of a varying yield, it is useful to define the “effective” oxygen yield, y_{eff} , as the yield that would be deduced if a system was assumed to behave as in the simplest model of chemical evolution (Edmunds 1990; Vila-Costa & Edmunds 1992)

$$y_{eff} = \frac{z_O}{\ln(\frac{1}{\mu})}. \quad (18)$$

Since we used the oxygen abundances given by number relative to hydrogen, while the value of z_O in Eq. (18) is given in units of mass fraction, the conversion for oxygen from Garnett et al. (1997) and Garnett (2002)

$$z_O = 12 \frac{O}{H} \quad (19)$$

was adopted.

5.1. The gas mass fractions

The gas fraction μ in a galaxy is estimated using the following standard relation:

$$\mu = \frac{M_{H_I} + M_{H_2}}{M_{H_I} + M_{H_2} + k L_B}, \quad (20)$$

where M_{H_I} is the mass of atomic hydrogen in the galaxy, M_{H_2} is the mass of molecular hydrogen in the galaxy (both M_{H_I} and M_{H_2} are corrected for the helium and heavy element contribution), L_B is the blue luminosity of the galaxy, and k is the mass-to-luminosity ratio. The mass of atomic hydrogen is derived in a standard way using the measured H I flux taken from literature and the adopted distance (Table A.1). If the mass of atomic hydrogen instead of the H I flux measurement is reported in literature, this value is rescaled to the adopted distance. The atomic hydrogen masses expressed in terms of M_{H_I}/L_B and corresponding references to the H I flux measurements are listed in Table 5 and Table 6.

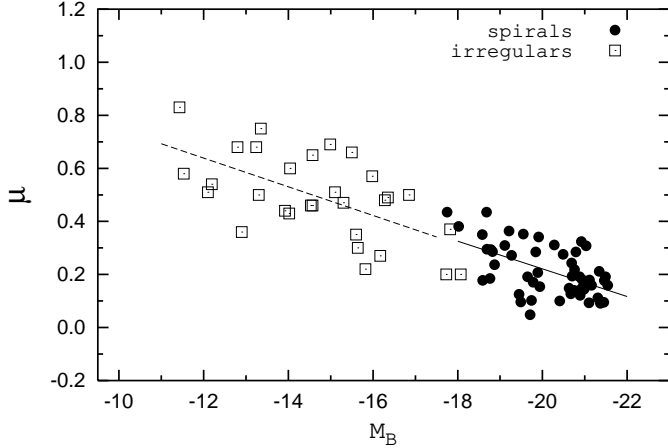


Fig. 12. Gas mass fraction as a function of the absolute blue magnitude M_B . The filled circles are spiral galaxies, the open squares are irregular galaxies. The solid line is the $\mu - M_B$ relationship for spiral galaxies, the dashed line is the $\mu - M_B$ relationship for irregular galaxies.

The mass of molecular hydrogen can only be estimated with indirect methods. The commonly accepted method is the use of the CO line flux and X conversion factor between the flux in the CO line and the amount of molecular hydrogen. The conversion factor $X = N(\text{H}_2)/I(\text{CO})$ strongly depends on the physical properties of the interstellar medium which are known to vary from galaxy to galaxy. The best-estimated values of the conversion factor for a sample of well-studied nearby galaxies span the range $0.6 \leq X \leq 10 \times 10^{20} \text{ mol cm}^{-2} (\text{K km s}^{-1})^{-1}$ (Boselli, Lequeux & Gavazzi 2002). The high values of the conversion factor correspond to low-luminosity irregular galaxies, and the low values of the conversion factor are found in spiral galaxies. Then the value of $X = 1 \times 10^{20} \text{ mol cm}^{-2} (\text{K km s}^{-1})^{-1}$ (including helium and heavy elements contribution) is adopted here for spiral galaxies. The molecular gas content is derived with this conversion factor using the measured CO flux from literature and distance (Table A.1). If the mass of molecular hydrogen instead of the CO flux measurement is reported in the literature, this value is rescaled to the adopted distance and adopted conversion factor. The molecular hydrogen masses expressed in terms of M_{H_2}/L_B and corresponding references to the CO flux measurements are given in Table 5 and Table 6.

The mass of the stellar component of the galaxy is estimated by converting the measured luminosity to mass via the mass-to-luminosity ratio. It is difficult to get a reliable estimation of the mass-to-luminosity ratio for individual galaxies. The μ and $\mu -$ dependent values will be used here only for examination of the general trends of these values with luminosity and rotation velocity but not for examination of individual galaxies. A similar investigation was carried out by Garnett (2002). He considered the impact of the choice of the mass-to-luminosity ratio on the trends by comparing the trends derived with the color-based mass-

to-luminosity ratio and constant mass-to-luminosity ratio. Garnett (2002) has found that the trends are fairly robust against the choice of mass-to-luminosity ratio. Based on this conclusion, a constant value of the mass-to-luminosity ratio $k = 1.5$ is adopted here for all spiral galaxies, and $k = 1$ is adopted for all irregular galaxies.

The derived values of the gas mass fraction in galaxies μ are listed in Table 5 (Col. 3). Unfortunately, for several spiral galaxies on our list no measurement of the CO flux is available. For these galaxies, the gas mass fraction is based on the atomic hydrogen mass only and is a lower limit. Taking into account that the average value is $M_{\text{H}_2}/M_{\text{H}_1} = 0.14$ (Boselli, Lequeux & Gavazzi 2002), one can hope that the use of a lower limit instead of the estimated value of gas fraction for several galaxies is quite acceptable.

The gas mass fraction in spiral galaxies as a function of absolute blue magnitude M_B is shown by the filled circles in Fig. 12. The solid line is the gas mass fraction – luminosity relationship (best fit determined via the least squares method) for spiral galaxies

$$\mu = 1.264 (\pm 0.220) + 0.0522 (\pm 0.0109) M_B. \quad (21)$$

The open squares in Fig. 12 are irregular galaxies. The dashed line is the gas fraction – luminosity relationship (best fit) for irregular galaxies

$$\mu = 1.289 (\pm 0.198) + 0.0542 (\pm 0.0134) M_B. \quad (22)$$

Comparison between Eq. (21) and Eq. (22) shows that the $\mu - M_B$ relationship for spiral galaxies coincides remarkably well with the $\mu - M_B$ relationship for irregular galaxies. It can also be seen in Fig. 12 that the gas mass fraction – luminosity relation for spiral galaxies is a direct continuation of the gas mass fraction – luminosity relationship for irregular galaxies.

5.2. The effective oxygen yields

The derived effective oxygen yields are presented as a function of absolute blue magnitude M_B in Fig. 13a and as a function of rotation velocity V_{rot} in Fig. 13b.

Inspection of Figs. 13a,b shows that there is only a hint of trends of the effective oxygen yield with luminosity and rotation velocity. The formal best fit to the $\log(y_{\text{eff}}) - M_B$ relation (solid line in Fig. 13a) is

$$\log y_{\text{eff}} = -2.834 (\pm 0.371) - 0.0120 (\pm 0.0183) M_B. \quad (23)$$

The mean value of the deviation of individual galaxies from the general trend is 0.13 dex. The formal best fit (least squares method) to data for spiral galaxies, the $\log(y_{\text{eff}}) - V_{\text{rot}}$ relation (solid line in Fig. 13b) is

$$\log y_{\text{eff}} = -2.698 (\pm 0.065) + 0.000496 (\pm 0.000321) V_{\text{rot}}. \quad (24)$$

The mean value of the deviation of individual galaxies from the general trend is 0.12 dex. The mean value of the effective oxygen yield in spiral galaxies is $y_{\text{eff}} = 0.00268$. The dashed line in Figs. 13a,b corresponds to the mean value of y_{eff} . Taking into account the large scatter of points

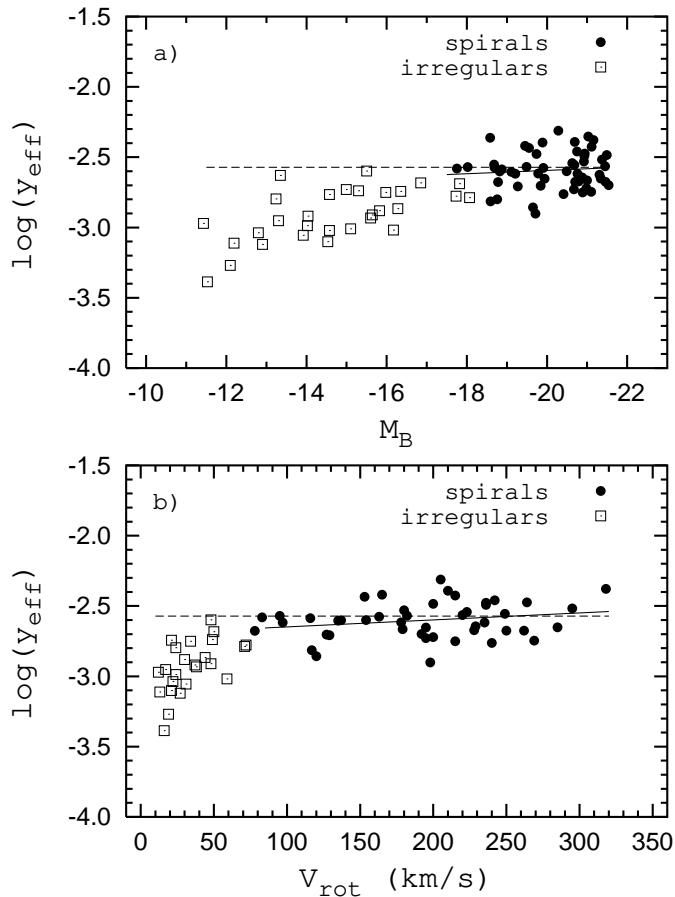


Fig. 13. (a) Effective oxygen yield as a function of the absolute blue magnitude M_B . The filled circles are spiral galaxies, the open circles are irregular galaxies. The solid line is the $y_{\text{eff}} - M_B$ relation for spiral galaxies (best fit). The dashed line corresponds to the mean $y_{\text{eff}} = 0.00268$ for spiral galaxies. (b) Effective oxygen yield as a function of the rotation velocity. Symbols are the same as in panel (a).

in the $\log(y_{\text{eff}}) - M_B$ and the $\log(y_{\text{eff}}) - V_{\text{rot}}$ diagrams, it is difficult to establish firmly how real are the trends of the effective oxygen yield in spiral galaxies with luminosity and rotation velocity. More accurate data are needed to confirm or reject these trends. Here we can only conclude that the effective oxygen yield in spiral galaxies remains approximatively constant.

It is widely accepted that the mass exchange (gas infall and/or galactic wind) between a galaxy and its environment plays a major role in the evolution of galaxies. Gas infall and galactic winds produce a shift of the position of a galaxy in the $\mu - \text{O}/\text{H}$ diagram towards lower oxygen abundances compared to the predictions of the closed-box models (see e.g. Mouhcine & Contini 2002). The location of spiral and irregular galaxies in the $\mu - \text{O}/\text{H}$ diagram together with the predictions of the closed-box model

$$z_O = y_O \ln\left(\frac{1}{\mu}\right) \quad (25)$$

are presented in Fig. 14a.

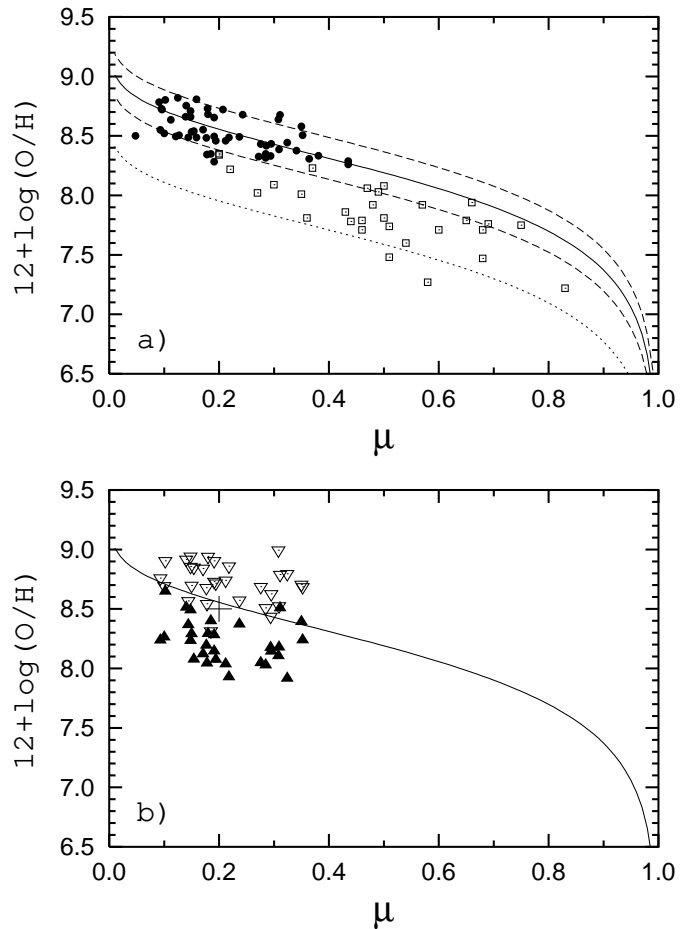


Fig. 14. (a) The positions of spiral (filled circles) and irregular (open squares) galaxies in the $\mu - \text{O}/\text{H}$ diagram together with the predictions of the closed-box models. The solid curve is the prediction of the closed-box model with oxygen yield $y_0 = 0.00268$ (the mean value of the effective oxygen yields derived for spiral galaxies). The dashed curves correspond to the predictions of the closed-box models with oxygen yields $y = 1.5 \times y_0$ and $y = y_0/1.5$. The dotted curve is the prediction of the closed-box models with oxygen yields $y = y_0/4$. (b) The oxygen abundances extrapolated to zero radius (open triangles) and extrapolated to the isophotal radius R_{25} (filled triangles) in spiral galaxies with well defined radial oxygen abundance gradients together with the $\mu - \text{O}/\text{H}$ track predicted by the closed-box model with oxygen yield $y_0 = 0.00268$. The large plus sign is the position of the solar vicinity region.

The solid line in Fig. 14a is the prediction of the closed-box model for the evolution of galaxies with oxygen yield $y_0 = y_{\text{eff}} = 0.00268$. As can be seen in Fig. 14a, the positions of spiral galaxies in the $\mu - \text{O}/\text{H}$ diagram are close to the track predicted by the closed-box model. The mean value of the O/H deviation of the individual galaxies from the closed-box model is 0.13 dex. The dashed lines in Fig. 14a correspond to the predictions of the closed-box models with oxygen yields $y = 1.5 \times y_0$ and $y = y_0/1.5$. The ma-

jority of spiral galaxies is located within the band defined by dashed lines.

It is well known that the closed-box model predicts many more low-metallicity stars than are observed in the solar neighbourhood, the so called ‘‘G-dwarf’’ paradox. Various versions of the infall model, in which an infall of gas onto the disk takes place for a long time, have been suggested (Tosi 1988a,b; Pagel & Tautvaišienė 1995; Pilyugin & Edmunds 1996a,b; Chiappini, Matteucci & Romano 2001; among many others) to explain the observed metallicity function. An infall model has also been applied to other spiral galaxies (Díaz & Tosi 1986; Mollá, Ferrini & Díaz 1996,1997; Pilyugin et al. 2002; Mouhcine & Contini 2002; Chiappini, Romano & Matteucci 2003). It is thus generally accepted that gas infall can play an important role in the chemical evolution of disks of spiral galaxies. Therefore, the fact that the positions of spiral galaxies are close to the position of the track of the closed-box model may appear surprising. It has been shown (Pilyugin & Ferrini 1998) that the present-day position of a system in the $\mu - O/H$ diagram is governed by its evolution in the recent past and is, in fact, independent of its evolution on long timescales. Therefore, the fact that the present-day position of spiral galaxies is close to the position of the closed-box model is not in conflict with the model, in which an infall of gas onto disk takes place for a long time (which is necessary to satisfy the observed abundance distribution function and the age – metallicity relation in the solar neighbourhood) since these observational data reflect the evolution of a system in the distant past. Of course, the simple model of chemical evolution of galaxies can be used only as the first-order approximation. To establish a more accurate relation between the present-day values of oxygen abundance and gas mass fraction in a galaxy, an appropriate model of chemical evolution should be developed (e.g. Pagel & Tautvaišienė 1995).

Inspection of Figs. 13a,b shows that the values of the effective oxygen yield in irregular galaxies are lower than that in spiral galaxies. The effective oxygen yield in irregular galaxies shows a clear trend with luminosity and rotation velocity. The positions of irregular galaxies in the $\mu - O/H$ diagram are systematically shifted towards lower oxygen abundances compared to the predictions of the closed-box model with oxygen yield y_0 typical for spiral galaxies. This suggests that the mass exchange between a galaxy and its environment (galactic winds) plays an important role in the chemical evolution of irregular galaxies. The dotted line in Fig. 14a corresponds to the closed-box models with oxygen yield $y = y_0/4$. Only two irregular galaxies from our sample are located below the dotted line. This implies that irregular galaxies lose only a moderate part of their manufactured heavy elements. Two facts are important: *i*) the smooth variation in gas mass fraction in spiral and irregular galaxies with luminosity over the full luminosity range, *ii*) the growth of effective oxygen yield with increasing luminosity from $M_B \sim -11$ to -18 which remains approximately constant for more luminous galaxies. These two facts taken together allow us to suggest

that the difference in the slopes of the $O/H - M_B$ relationships for spiral and irregular galaxies is real and that the variation of the effective oxygen yield with luminosity is responsible for the bend in the luminosity – metallicity relationship.

How realistic is the value of the mean oxygen yield derived here for spiral galaxies? Fig. 14b shows the oxygen abundances extrapolated to zero radius in spiral galaxies together with the $\mu - O/H$ track predicted by the closed-box model with the derived oxygen yield. One can expect that the central oxygen abundances in the most evolved spiral galaxies correspond to the oxygen abundance when the system had exhausted the gas. As can be seen in Fig. 14b, the upper limit of the central oxygen abundances in spiral galaxies is close to the oxygen abundances predicted by the model with derived oxygen yield when the gas mass fraction is close to zero. The present-day oxygen abundance at the solar galactocentric distance in our Galaxy is about $12 + \log(O/H) = 8.50$ as traced by H II regions (Rodríguez 1999; Caplan et al. 2000; Deharveng et al. 2000; Pilyugin, Ferrini & Shkvarun 2003) and derived from the interstellar absorption lines towards the stars (Meyer, Jura & Cardelli 1998; Sofia & Meyer 2001), and for the present-day gas mass fraction, 0.15 – 0.20 appears to be a reasonable value (Malinie et al. 1993). As shown in Fig. 14b, the position of the solar vicinity (large plus sign) is close to the $\mu - O/H$ track predicted by the closed-box model with derived oxygen yield. Thus, the data in Fig. 14b imply that the value of the oxygen abundance derived here is quite realistic.

It should be noted that the value of the oxygen yield is derived here on the basis of gas-phase oxygen abundances. Some fraction of the oxygen is locked into dust grains in H II regions. Meyer, Jura & Cardelli (1998) obtained a limit to the dust-phase oxygen abundance in the interstellar medium in the vicinity of the Sun. Assuming various mixtures of oxygen-bearing grain compounds, they found that it is difficult to increase the oxygen dust fraction beyond ~ 0.14 dex, simply because the requisite metals are far less abundant than oxygen. Esteban et al. (1998) found that the fraction of the dust-phase oxygen abundance in the Orion nebula is about 0.1 dex. Thus, the true value of the oxygen yield is slightly higher than the value obtained here and is around $y = 0.003$.

6. Comparison with previous studies

How reliable are the results obtained here? How significant is the difference between the P-based and the R_{23} -based $O/H - M_B$ relationships? The validity of the oxygen abundances obtained here can be tested by a comparison with the T_e -based oxygen abundances determined recently in the disk of the galaxy NGC 5457 by Kennicutt, Bresolin & Garnett (2003). It is worth noting that the comparison of oxygen abundances derived through the P-method and through the T_e -method has already been made for the galaxy NGC 5457 (Pilyugin 2001b), as well as for the Milky Way (Pilyugin, Ferrini & Shkvarun 2003), and

for a sample of star-forming emission-line galaxies from the KPNO International Spectroscopic Survey (KISS) (Melbourne et al. 2004). A good agreement has been found in all cases. Recently Kennicutt, Bresolin & Garnett (2003) obtained new spectra for a number of H II regions in the disk of the galaxy NGC 5457 and determined the T_e -based abundances. They compared their temperature-based abundances with those derived for the same H II regions using different calibrations. According to their Fig. 14, the validity of the P-based abundances is questionable. The data from Kennicutt, Bresolin & Garnett (2003) have been used here to test the validity of the P-calibration as well as other popular calibrations. To enlarge the comparison we have also included direct abundance measurements of H II regions in this galaxy from the literature (the compilation of the spectral data was performed by Pilyugin 2001b) as well as direct abundance measurements of H II regions in other galaxies (compilation from Pilyugin 2001a).

Fig. 15a shows the $O/H_P - O/H_{T_e}$ diagram (the analog of Fig.14 from Kennicutt, Bresolin & Garnett 2003). The filled circles are direct abundance measurements of H II regions in the galaxy NGC 5457 with $12+\log O/H_{T_e} > 8.2$ from Kennicutt, Bresolin & Garnett (2003). The filled triangles are direct abundance measurements of H II regions in this galaxy from other authors (compilation from Pilyugin 2001b) The open squares are direct abundance measurements of H II regions in other galaxies (compilation from Pilyugin 2001a). Fig. 15a shows that there is a satisfactory agreement between O/H_{T_e} and O/H_P abundances. The origin of the disagreement between Kennicutt et al's and our conclusions is evident. The relationship between oxygen abundance and strong oxygen line intensities is double-valued with two distinct parts usually known as the “lower” and “upper” branches of the $R_{23} - O/H$ relationship. The high-metallicity P-calibration is valid only for H II regions which belong to the upper branch, i.e. with $12+\log(O/H)$ higher than ~ 8.2 . The unjustified use of the high-metallicity P-calibration in the determination of the oxygen abundance in low-metallicity H II regions results in overestimated P-based oxygen abundances (Pilyugin 2003a). Our $O/H_P - O/H_{T_e}$ diagram (Fig. 15a) shows only the high-metallicity H II regions with $12+\log O/H_{T_e} > 8.2$. On the contrary, Fig.14 of Kennicutt, Bresolin & Garnett (2003) also includes low-metallicity H II regions, with $12+\log(O/H)$ lower than ~ 8.2 . They do not belong to the upper branch, and, as a consequence, the high-metallicity P-calibration cannot be used in the determination of the oxygen abundance in these H II regions. This is the reason why the low-metallicity H II regions in the galaxy NGC 5457 are not presented in our Fig. 15a and are excluded from the analysis above (see Sect. 2).

Fig. 15b shows the O/H_{ZKH} versus $(O/H)_{T_e}$ diagram for the same sample of H II regions as in Fig. 15a. The O/H_{ZKH} abundances are derived using the high-metallicity calibration from Zaritsky, Kennicutt & Huchra (1994). Zaritsky et al.'s calibration is an average of the three calibrations by Edmunds & Pagel (1994), McCall

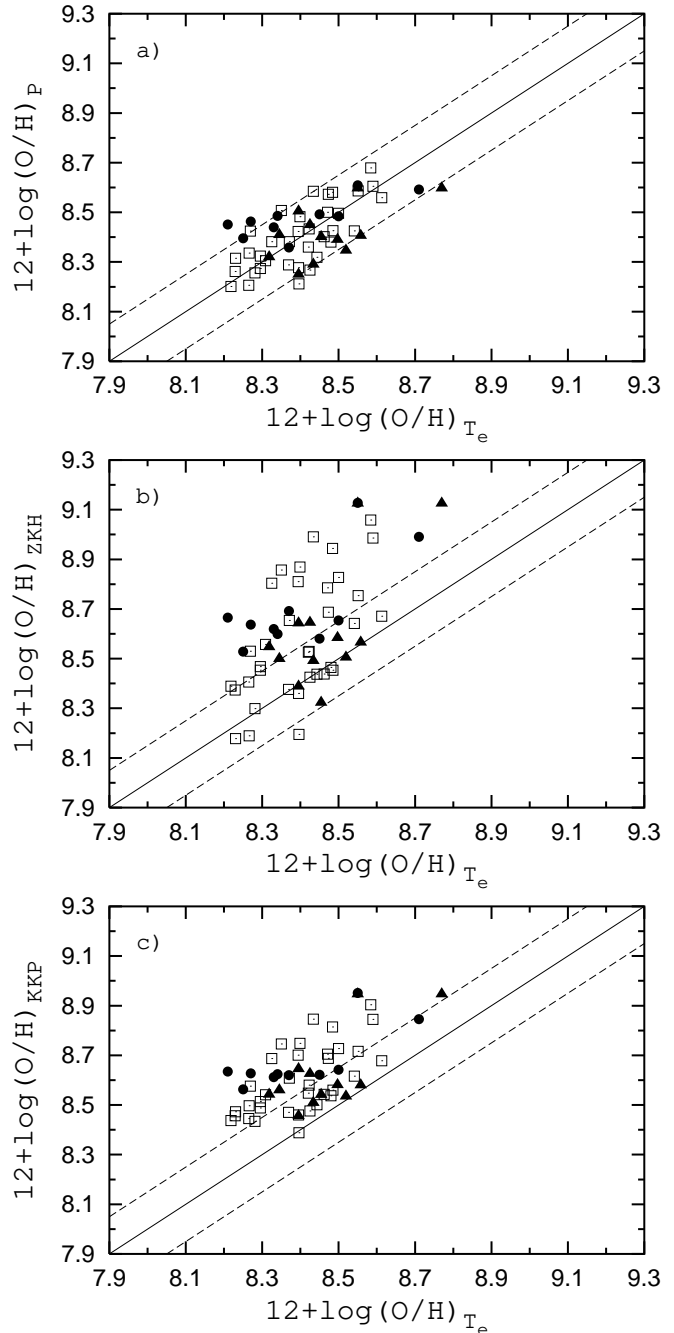


Fig. 15. Comparison of temperature-based oxygen abundances O/H_{T_e} with those derived with different calibrations for high-metallicity H II regions. (a) The $O/H_P - O/H_{T_e}$ diagram. The filled circles represent the O/H_{T_e} abundances for H II regions in the galaxy NGC 5457 from Kennicutt, Bresolin & Garnett (2003), the filled triangles are the O/H_{T_e} abundances for H II regions in this galaxy from other authors. The open squares are the O/H_{T_e} abundances for H II regions in other galaxies. The O/H_P abundances are derived through the high-metallicity P-calibration. The solid line is the equal-value line, the dashed lines are shifted by $+0.15$ dex and -0.15 dex. (b) The $O/H_{ZKH} - O/H_{T_e}$ diagram for the same H II regions. The O/H_{ZKH} abundances are derived using the high-metallicity calibration from Zaritsky, Kennicutt & Huchra (1994). (c) The $O/H_{KKP} - O/H_{T_e}$ diagram for the same H II regions. The O/H_{KKP} abundances are derived using the high-metallicity calibration from Kobulnicky,

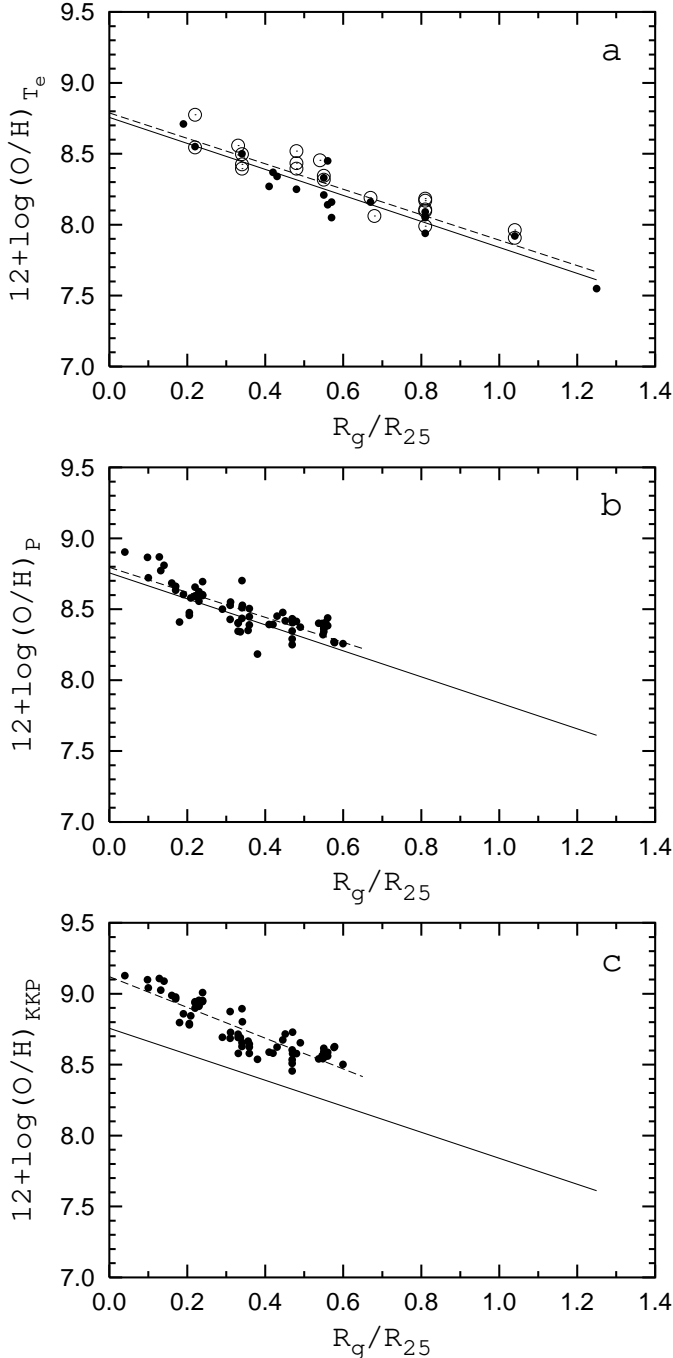


Fig. 16. The oxygen abundance versus galactocentric distance for the galaxy NGC 5457. (a) The filled circles are temperature-based abundances from Kennicutt, Bresolin & Garnett (2003). The solid line is the least squares fit to these data. The open circles are temperature-based abundances from other authors (compilation from Pilyugin 2001b). The dashed line is the least squares fit to all the temperature-based abundances. (b) The filled circles are oxygen abundances derived through the high-metallicity P-calibration for a large sample of H II regions with $R_g < 0.60R_{25}$. The best fit to these data is presented by the dashed line. The solid line is the same as in (a). (c) The filled circles are abundances derived using the calibration from Kobulnicky, Kennicutt & Pizagno (1999) for the same H II regions. The least squares fit to these data is presented by the dashed line.

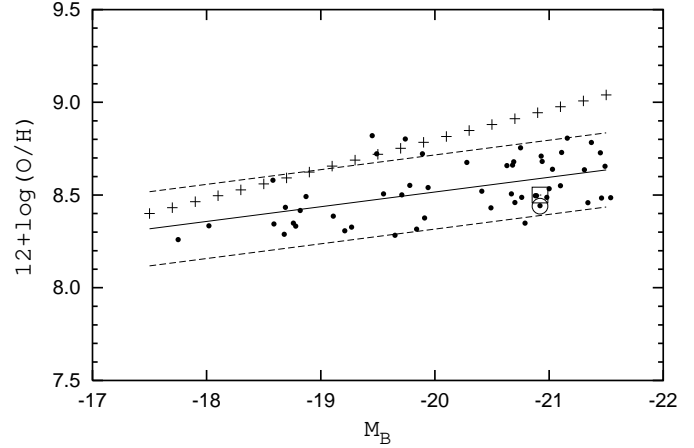


Fig. 17. The characteristic oxygen abundance as a function of absolute blue magnitude M_B for our sample of spiral galaxies (the filled circles). The solid line is the $O/H - M_B$ relationship (best fit derived through the least squares method). The dashed lines correspond to the lines shifted by -0.2 dex and $+0.2$ dex along the vertical axes relatively to the derived $O/H - M_B$ relationship. The oxygen abundances in the galaxy NGC 5457 are presented by the open circle (O/H at $R = 0.4R_{25}$) and open square (O/H at the disk half-light radius). The $O/H - M_B$ relationship from Garnett (2002) is shown by plus signs.

et al. (1985), and Dopita & Evans (1986), hence this calibration can be considered as “representative” for one-dimensional calibrations. Fig. 15c shows the O/H_{KKP} versus $(O/H)_{T_e}$ diagram for the same sample of H II regions as in Fig. 15a. The O/H_{KKP} abundances are derived using the two-dimensional high-metallicity calibration from Kobulnicky, Kennicutt & Pizagno (1999). Fig. 15a-c shows that the O/H_P abundances agree significantly better with the O/H_{T_e} abundances than do the $(O/H)_{ZKH}$ and $(O/H)_{KKP}$ abundances.

We assume that the temperature-based abundance is the “true” abundance and that the difference between, e.g. the P-based abundance and the T_e -based abundance is due only to the error attached to the P-based abundance. However, the O/H_{T_e} abundances determined by Kennicutt, Bresolin & Garnett (2003) in H II regions of the galaxy NGC 5457 with close galactocentric distances ($0.55R_{25} \leq R_g \leq 0.57R_{25}$) show a large scatter, from $12+\log(O/H)_{T_e} = 8.05$ for H II region H71 to $12+\log(O/H)_{T_e} = 8.45$ for H II region H128. This may be evidence for large uncertainty in O/H_{T_e} abundances. If this is the case, the uncertainty in the O/H_{T_e} abundances can make an appreciable contribution to the disagreement between the P-based and the T_e -based abundances.

It is worth noting that the direct comparison of temperature-based oxygen abundances O/H_{T_e} with those derived with different calibrations is affected by the selection criteria. Indeed, in the high metallicity range, the weak temperature-sensitive line $O[III]\lambda 4363$ is usually measured in high-excitation H II regions. It is known that

the disagreement between temperature-based abundances and those derived with one-dimensional R_{23} calibrations is lowest for high-excitation H II regions and is larger for low-excitation H II regions, while the P-based abundances agree with the T_e -based abundances both for high- and low-excitation H II regions. Since the two-dimensional calibration of Kobulnicky, Kennicutt & Pizagno (1999) converts, in fact, into one-dimensional calibration at high metallicities, one can expect that the mean value of the disagreement between O/H_{KKP} and $(O/H)_{T_e}$ abundances is larger than for the sample of high-excitation H II regions in Fig. 15c. This statement can be checked through comparing the radial gradients traced by oxygen abundances derived using different methods. This also provides additional verification of the validity of oxygen abundances derived through different methods.

The O/H_{T_e} abundances versus galactocentric distance for the galaxy NGC 5457 are shown in Fig. 16a. The small filled circles are the data from Kennicutt, Bresolin & Garnett (2003). The best fit to these data

$$12 + \log(O/H)_{T_e,KBG} = 8.76 (\pm 0.06) - 0.90 (\pm 0.08) \times (R/R_{25}) \quad (26)$$

is shown by the solid line. The open circles are O/H_{T_e} abundances from other authors (compilation from Pilyugin 2001b). The best fit to all data

$$12 + \log(O/H)_{T_e,all} = 8.79 (\pm 0.04) - 0.90 (\pm 0.06) \times (R/R_{25}) \quad (27)$$

is shown by the dashed line. Fig. 16a, as well as the comparison between Eq. (26) and Eq. (27), shows that the O/H_{T_e} abundances from Kennicutt, Bresolin & Garnett (2003) are slightly shifted towards lower abundances compared to those from other authors.

Fig. 16b shows the oxygen abundances derived here using the P-calibration for a large (65) sample of H II regions with $R_g > 0.6R_{25}$. The least squares fit to these data

$$12 + \log(O/H)_P = 8.79 (\pm 0.03) - 0.88 (\pm 0.08) \times (R/R_{25}) \quad (28)$$

is shown in Fig. 16b by the dashed line. The $O/H_{T_e} - R_g$ relationship of Kennicutt, Bresolin & Garnett (2003) is shown by the solid line. Fig. 16b, as well as the comparison between Eq. (26), Eq. (27) and Eq. (28), shows that there is a very good agreement, both in the zero point and slope, between the radial O/H_{T_e} abundance gradient and the O/H_P abundance gradient in the disk of the galaxy NGC 5457.

Fig. 16c shows the radial distribution of the O/H_{KKP} abundances, derived using the high-metallicity calibration from Kobulnicky, Kennicutt & Pizagno (1999), for the sample of H II regions from Fig. 16b. The least squares fit to these data

$$12 + \log(O/H)_{KKP} = 9.12 (\pm 0.03) - 1.08 (\pm 0.07) \times (R/R_{25}) \quad (29)$$

is shown in Fig. 16c by the dashed line. The $O/H_{T_e} - R_g$ relationship of Kennicutt, Bresolin & Garnett (2003) is shown by the solid line. Fig. 16c, as well as the comparison between Eq. (26), Eq. (27) and Eq. (29), clearly shows that the central oxygen abundance in NGC 5457, derived using the calibration from Kobulnicky, Kennicutt & Pizagno (1999), is overestimated (by a factor ~ 2) in comparison with the one derived with the T_e and P-methods. The slopes of the $(O/H)_{T_e}$ -based and the $(O/H)_{R_{23}}$ -based gradients are significantly different.

According to Garnett et al. (1997), the radial oxygen abundance gradient within the disk of NGC 5457 with oxygen abundances derived through the R_{23} -calibration is

$$12 + \log(O/H)_{R_{23}} = 9.13 - 1.36 \times (R/R_{25}). \quad (30)$$

Comparison between Eq. (26), Eq. (27) and Eq. (30) clearly shows that the central oxygen abundance in NGC 5457, derived using the R_{23} calibration, is overestimated (by a factor ~ 2) in comparison with the one derived with the T_e and P-methods. The slopes of the $(O/H)_{T_e}$ -based and the $(O/H)_{R_{23}}$ -based gradients are significantly different.

There is thus a very good agreement, both in the zero point and slope, between the radial O/H_{T_e} abundance gradient and the O/H_P abundance gradient within the disk of the galaxy NGC 5457. For radial distributions of abundances derived with other calibrations, both the central oxygen abundances and the slopes do not agree with $(O/H)_{T_e}$ -based values. This strongly supports our claim that the O/H_P abundances are significantly more realistic than abundances derived with other calibrations.

The temperature-based characteristic oxygen abundance in the galaxy NGC 5457 can also be used as the "Rosetta Stone" to test the validity of the $O/H - M_B$ relationship obtained here. The characteristic oxygen abundance as a function of absolute blue magnitude M_B for our sample of spiral galaxies is presented in Fig. 17. The positions of individual galaxies (points) and the $O/H - M_B$ relationship (solid line) are the same as in in Fig. 6. The dashed lines correspond to the lines shifted by -0.2 dex and $+0.2$ dex along the vertical axes relatively to the derived $O/H - M_B$ relationship. The oxygen abundances in the galaxy NGC 5457 are presented by the open circle (O/H at $R = 0.4R_{25}$) and open square (O/H at the disk half-light radius). The line shown by plus signs in Fig. 17 is the luminosity - metallicity relationship for spiral galaxies obtained by Garnett (2002). Fig. 17 shows that there is a large difference between the luminosity - metallicity relationship derived here and that from Garnett (2002). The main reason of this discrepancy is due to the fact that our luminosity - metallicity relationship is based on the oxygen abundances derived through the P-calibration while Garnett has used oxygen abundances derived through the R_{23} -calibrations. The recent results on the oxygen abundance determination in the disk of the well-studied spiral galaxy NGC 5457 (M 101) provide a possibility to check the credibility of these relationships. Kennicutt, Bresolin

& Garnett (2003) derived the radial distribution of the oxygen abundance in the disk of NGC 5457, traced by the H II regions with oxygen abundances derived with the classical T_e – method. The characteristic oxygen abundance (as adopted here the oxygen abundance at $R = 0.4R_{25}$) in the galaxy NGC 5457 is presented by the open circle in Fig. 17. It is evident that the T_e -based characteristic oxygen abundances in the galaxy NGC 5457 are in conflict with Garnett’s luminosity – metallicity relationship but agree with our luminosity – metallicity relationship. It is not surprising since it was shown above that there is a very good agreement, both in the zero point and slope, between our P-based oxygen abundance distribution, Eq. (28), and the T_e -based oxygen abundance distribution, Eq. (26), of Kennicutt, Bresolin & Garnett (2003), while the R_{23} -based oxygen abundance distribution, Eq. (30), of Garnett et al. (1997) is quite different. It should be noted that Garnett (2002) used the oxygen abundances at the disk half-light radius to built the luminosity – metallicity relationship. Can this make a significant contribution to the deviation of the characteristic oxygen abundance in the galaxy NGC 5457 from the luminosity – metallicity relationships based on oxygen abundances at the disk half-light radius? Based on Garnett’s conclusion: “for comparison, I include results based on using the value of O/H at one disk scale length; this change has little effect on the overall results”, one can expect that the difference in the choice of the “characteristic” radius plays a minor role. For verification and illustration, the T_e -based oxygen abundance in the galaxy NGC 5457 at the disk half-light radius (equal to 1.685 times the exponential scale length) is obtained and presented in Fig. 17 by the open square. Fig. 17 shows that using the characteristic oxygen abundance at $R = 0.4R_{25}$ in the galaxy NGC 5457 instead of the value of O/H at the disk half-light radius has little effect on the overall result. Thus, the T_e -based characteristic oxygen abundances in the galaxy NGC 5457 are in conflict with the luminosity – metallicity relationship derived by Garnett (2002) with the R_{23} -based oxygen abundances, but agree with our luminosity – metallicity relationship derived with the P-based oxygen abundances.

7. Conclusions

We performed a compilation of more than 1000 published spectra of H II regions in 54 spiral galaxies. The oxygen and nitrogen abundances in each H II region were recomputed in a homogeneous way, using the P–method. The radial distributions of the oxygen abundances, nitrogen abundances, and nitrogen-to-oxygen abundance ratios were derived. The parameters of the radial distributions (the extrapolated central intersect value and the gradient) are listed.

The correlations between oxygen abundance and macroscopic properties of galaxies are examined. The oxygen abundance in the disk of a galaxy at $r = 0.4R_{25}$, where R_{25} is the isophotal radius, is used as a characteristic (or representative) oxygen abundance for spiral galaxies. We

found that the oxygen abundance in spiral galaxies correlates with its luminosity, rotation velocity, and morphological type: the correlation with the rotation velocity may be slightly tighter.

There is a significant difference between the luminosity – metallicity relationship derived here and that based on the oxygen abundances derived through the R_{23} –calibrations. The T_e -based characteristic oxygen abundances in the galaxy NGC 5457 (Kennicutt, Bresolin & Garnett 2003) agree with our luminosity – metallicity relationship derived with the P-based oxygen abundances but is in conflict with the luminosity – metallicity relationship derived by Garnett (2002) with the R_{23} -based oxygen abundances.

The derived luminosity – metallicity relation for spiral galaxies is compared to that for irregular galaxies. We found that the slope of the oxygen abundance – luminosity relationship for spirals is slightly more shallow than the one for irregular galaxies.

The effective oxygen yields were derived for spiral and irregular galaxies. We found that the effective oxygen yield increases with increasing luminosity from $M_B \sim -11$ to $M_B \sim -18$ (or with increasing rotation velocity from $V_{\text{rot}} \sim 10 \text{ km s}^{-1}$ to $V_{\text{rot}} \sim 100 \text{ km s}^{-1}$) and then remains approximately constant. Irregular galaxies from our sample have effective oxygen yields lowered by a factor of 3 at maximum, i.e. irregular galaxies usually retain at least 1/3 of the oxygen they manufactured during their evolution. From the comparison between the effective oxygen yields for spiral and irregular galaxies (with R_{23} -based oxygen abundances in spiral galaxies), Garnett (2002) found however that an irregular galaxy can lose up to 90% ÷ 95% of the oxygen manufactured.

Acknowledgements. We thank Prof. B.E.J. Pagel for a careful reading of the manuscript and useful comments and suggestions which helped to improve the paper. We thank the anonymous referee for helpful comments. This study was supported by the sabbatical grant SAB2001-0165 of the Spanish Ministerio de Educación, Cultura y Deporte (L.S.P.) and by the Ukrainian Fund of Fundamental Investigation, grant No 02.07/00132 (L.S.P.).

References

- Alloin, D., Collin-Souffrin, S., Joly, M. & Vigroux, L. 1979, *A&A*, 78, 200
- Alloin, D., Edmunds, M.G., Lindblad, P.O. & Pagel, B.E.J. 1981, *A&A*, 101, 377
- Alves, D.R. & Nelson, C.A. 2000, *ApJ*, 542, 789
- Amram, P., Marcelin, M., Balkowski, C., Cayatte, V., Sullivan, W.T. & Le Coarer, E. 1994, *A&AS*, 103, 5
- Appleton, P.N., Davies, R.D. & Stephenson, R.J. 1981, *MNRAS*, 195, 327
- Bajaja, E. & Martin, M.C. 1985, *AJ*, 90, 1783
- Bajaja, E., Wielebinski, R., Reuter, H.-P., Harnett, J.I. & Hummel, E. 1995, *A&AS*, 114, 147
- Becker, R., Mebold, U., Reif, K. & van Woerden, H. 1988, *A&A*, 203, 21

- Begeman, K.G., Broeils, A.H. & Sanders, R.H. 1991, *MNRAS*, 249, 523
- Blair, W.P., Kirshner, R.P. & Chevalier, R.A. 1982, *ApJ*, 254, 50
- Bosma, A. 1981, *AJ*, 86, 1791
- Bosma, A., Casini, C., Heidmann, J., van der Hulst, J.M. & van Woerden, H. 1980, *A&A*, 89, 345
- Bosma, A., van der Hulst, J.M. & Sullivan, W.T. 1977, *A&A*, 57, 373
- Bravo-Alfaro, H., Szomoru, A., Cayatte, V., Balkowski, C. & Sancisi, R. 1997, *A&AS*, 126, 537
- Bresolin, F. & Kennicutt, R.C. 2002, *ApJ*, 572, 838
- Bresolin, F., Kennicutt, R.C. & Garnett, D.R. 1999, *ApJ*, 510, 104
- Broeils, A.H. & Rhee, M.-H. 1997, *A&A*, 324, 877
- Buta, R. 1988, *ApJS*, 66, 233
- Caplan, J., Deharveng, L., Peña, M., Costero, R. & Blondel, C. 2000, *MNRAS*, 311, 328
- Caputo, F., Marconi, M. & Musella, I. 2002, *ApJ*, 566, 833
- Carignan, C., Charbonneau, P., Boulanger, F. & Viallefond, F. 1990, *A&A*, 234, 43
- Carignan, C. & Puche, D. 1990, *AJ*, 100, 394
- Carollo, C.M. & Lilly, S.J. 2001, *ApJL*, 548, L153
- Castellanos, M. 2000, Ph.D., Madrid
- Castellanos, M., Díaz, A.I. & Terlevich, E. 2002, *MNRAS*, 329, 315
- Casertano, S. & van Gorkom, J.H. 1991, *AJ*, 101, 1231
- Chiappini, C., Matteucci, F. & Romano, D. 2001, *ApJ*, 554, 1044
- Chiappini, C., Romano, D. & Matteucci, F. 2003, *MNRAS*, 339, 63
- Christensen, T., Petersen, L. & Gammelgaard, P. 1997, *A&A*, 322, 41
- Ciardullo, R., Feldmeier, J.J., Jacoby, G.H., et al. 2002, *ApJ*, 577, 31
- Considère, S., Coziol, R., Contini, T. & Davoust, E. 2000, *A&A*, 356, 89
- Corbelli, E. & Salucci, P. 2000, *MNRAS*, 311, 441
- Côté, S., Carignan, C. & Freeman, K.C. 2000, *AJ*, 120, 3027
- Cox, P. & Downes, D. 1996, *ApJ*, 473, 219
- Davidge, T.J. 1998, *ApJ*, 497, 650
- Dean, J.F. & Davies, R.D. 1975, *MNRAS*, 170, 503
- Deharveng, L., Caplan, J., Lequeux, J., Azzopardi, M., Breysacher, J., Tarenghi, M. & Westerlund, B. 1988, *A&AS*, 73, 407
- Deharveng, L., Peña, M., Caplan, J. & Costero, R. 2000, *MNRAS*, 311, 329
- de Blok, W.J.G. & Bosma, A. 2002, *A&A*, 385, 816
- Dennefeld, M. & Kunth, D. 1981, *AJ*, 86, 989
- de Vaucouleurs, G. 1979, *ApJ*, 227, 729
- de Vaucouleurs, G., de Vaucouleurs, A., Corvin, H.G., Buta, R.J., Paturel, J. & Fouque, P. 1991, *Third Reference Catalog of bright Galaxies*(New York: Springer) (RC3)
- de Vaucouleurs, G., Pence, W.D. & Davoust, E. 1983, *ApJS*, 53, 17
- Díaz, A.I., Terlevich, E., Pagel, B.E.J., Vílchez, J.M. & Edmunds, M.G. 1987, *MNRAS*, 226, 19
- Díaz, A.I., Terlevich, E., Vílchez, J.M., Pagel, B.E.J. & Edmunds M.G. 1991, *MNRAS*, 253, 245
- Díaz, A.I. & Tosi, M. 1986, *A&A*, 158, 60
- d'Odorico, S., Rosa, M. & Wampler, E.J. 1983, *A&A*, 53, 97
- Dopita, M.A. & Evans, I.N. 1986, *ApJ*, 307, 431
- Drozdovsky, I.O. & Karachentsev, I.D. 2000, *A&AS*, 142, 425
- Dufour, R.J., Talbot, R.J., Jensen, E.B. & Shields G.A. 1980, *ApJ*, 236, 119
- Eastman, R.G., Schmidt, B.P. & Kirshner, R. 1996, *ApJ*, 466, 911
- Edmunds, M.G. 1990, *MNRAS*, 246, 678
- Edmunds, M.G. & Pagel, B.E.J. 1984, *MNRAS*, 211, 507
- Ekholm, T., Lanoix, P., Teerikorpi, P., Fouqué, P. & Paturel, G. 2000, *A&A*, 355, 835
- Elmegreen, D.M. & Salzer, J.J. 1999, *AJ*, 117, 764
- Esteban, C., Peimbert, M., Torres-Peimbert, S. & Escalante, V. 1998, *MNRAS*, 295, 401
- Federspiel, M., Tammann, G.A. & Sandage, A. 1998, *ApJ*, 495, 115
- Feldmeier, J.J., Ciardullo, R. & Jacoby, G.H. 1997, *ApJ*, 479, 231
- Ferguson, A.M.N., Gallagher, J.S. & Wyse R.F.G. 1998, *AJ*, 116, 673
- Ferrarese, L., Ford, H.C., Huchra, J., et al. 2000, *ApJS*, 128, 431
- Fierro, J., Torres-Peimbert, S. & Peimbert, M. 1986, *PASP*, 98, 1032
- Fouqué, P., Bottinelli, L., Gouguenheim, L. & Paturel, G. 1990, *ApJ*, 349, 1
- Freedman, W.L., Madore, B.F., Gibson, B.K., et al. 2001, *ApJ*, 553, 47
- Garcia, A.M. 1993, *A&AS*, 100, 47
- García-Barreto, J.A., Downes, D. & Huchtmeier, W.K. 1994, *A&A*, 288, 705
- Garnett, D.R. 1992, *AJ*, 103, 1330
- Garnett, D.R. 2002, *ApJ*, 581, 1019
- Garnett, D.R., Kennicutt, R.C. & Bresolin, F. 2004, *ApJ*, 607, L21
- Garnett, D.R., Odewanh, S.C. & Skillman, E.D. 1992, *AJ*, 104, 1714
- Garnett, D.R. & Shields, G.A. 1987, *ApJ*, 317, 82
- Garnett, D.R., Shields, G.A., Peimbert, M., Torres-Peimbert, S., Skillman, E.D., Dufour, R.J., Terlevich, E. & Terlevich, R.J. 1999, *ApJ*, 513, 168
- Garnett, D.R., Shields, G.A., Skillman, E.D., Sagan, S.P. & Dufour, R.J. 1997, *ApJ*, 489, 63
- Gavazzi, G., Boselli, A., Scodreggio, M., Pierini, D. & Belsole, E. 1999, *MNRAS*, 304, 595
- Gibson, B.K. & Stetson, P.B. 2001, *ApJL*, 547, L103
- Guélin, M. & Weliachew, L. 1970, *A&A*, 7, 141
- Guhathakurta, P., van Gorkom, J.H., Kotanyi, C.G. & Balkowski, C. 1988, *AJ*, 96, 851
- Haynes, M.P., Hogg, D.E., Maddalena, R.J., Roberts, M.S. & van Zee, L. 1998, *AJ*, 115, 62
- Heckman, T.M., Balick, B. & Sullivan, W.T. 1978, *ApJ*, 224, 745
- Helfer, T.T. & Blitz, L. 1995, *ApJ*, 450, 90
- Helfer, T.T., Thornley, M.D., Regan, M.W., et al. 2003, *ApJS*, 145, 259
- Henry, R.B.C., Balkowski, C., Cayatte, V., Edmunds, M.G. & Pagel, B.E.J. 1996, *MNRAS*, 283, 635
- Henry, R.B.C., Pagel, B.E.J. & Chincarini, G.L. 1994, *MNRAS*, 266, 421
- Henry, R.B.C., Pagel, B.E.J., Lasseter, D.F. & Chincarini G.L. 1992, *MNRAS*, 258, 321
- Herrnstein, J.R., Moran, J.M., Greenhill, L.J., et al. 1999, *Nature*, 400, 539
- Hewitt, J.N., Haynes, M.P. & Giovanelli, R. 1983, *AJ*, 88, 272
- Ho, L.C., Filippenko, A.V. & Sargent, W.L.W. 1997, *ApJS*, 112, 315

- Hoekstra, H., van Albada, T.S. & Sancisi, R. 2001, MNRAS, 323, 453
- Hoffman, G.L., Salpeter, E.E., Farhat, B., Roos, T., Williams, H. & Helou, G. 1996, ApJS, 105, 269
- Huchtmeier, W.K. 1975, A&A, 45, 259
- Huchtmeier, W.K. & Richter, O.G. 1986a, A&AS, 63, 323
- Huchtmeier, W.K. & Richter, O.G. 1986b, A&AS, 64, 111
- Huchtmeier, W.K. & Seiradakis, J.H. 1985, A&A, 143, 216
- Hunter, D.A., Rubin, V.C. & Gallagher, J.S. 1986, AJ, 91, 1086
- Jacoby, G.H., Ciardullo, R., Booth, J. & Ford, H.C. 1989, ApJ, 344, 704
- Jensen, J.B., Tonry, J.L., Barris, B.J., et al. 2003, ApJ, 583, 712
- Jörsäter, S. & van Moorsel, G.A. 1995, AJ, 110, 2037
- Joshi, Y.C., Pandey, A.K., Narasimha, D., Sagar, R. & Giraud-Héraud, Y. 2003, A&A, 402, 113
- Jurcic, J.S., Pierce, M.J. & Jacoby, G.H. 2000, MNRAS, 313, 868
- Karachentsev, I.D. & Drozdovsky, I.O. 1998, A&AS, 131, 1
- Karachentsev, I.D., Makarov, D.I. & Huchtmeier, W.K. 1999, A&AS, 139, 97
- Karachentsev, I.D., Makarov, D.I., Sharina, M.E., et al. 2003a, A&A, 398, 479
- Karachentsev, I.D., Sharina, M.E., Dolphin, A.E., et al. 2003b, A&A, 398, 467
- Karachentsev, I.D. & Tikhonov, N.A. 1993, A&AS, 100, 227
- Kenney, J.D. & Young, J.S. 1988, ApJS, 66, 261
- Kennicutt, R.C., Bresolin, F. & Garnett, D.R. 2003, ApJ, 591, 801
- Kennicutt, R.C. & Garnett, D.R. 1996, ApJ, 456, 504
- Kewley, L.J. & Dopita, M.A. 2002, ApJS, 142, 35
- Kim, M., Kim, E., Lee, M.G., Sarajedini, A. & Geisler, D. 2002, AJ, 123, 244
- Kinkel, U. & Rosa, M.R. 1994, A&A, 282, L37
- Kinman, T.D. & Davidson, K. 1981, ApJ, 243, 127
- Kobulnicky, H.A., Kennicutt, R.C. & Pizano J.L. 1999, ApJ, 514, 544
- Koper, E., Dame, T.M., Israel, F.P. & Thaddeus, P. 1991, ApJ, 383, L11
- Kraan-Korteweg, R.C., Cameron, L.M. & Tammann, G.A. 1988, ApJ, 331, 620
- Krumm, N. & Salpeter, E.E. 1979, AJ, 84, 1138
- Kuno, N. & Nakai, N. 1997, PASJ, 49, 279
- Kwitter, K.B. & Aller, L.H. 1981, MNRAS, 195, 939
- Lamareille, F., Mouhcine, M., Contini, T., Lewis, I., Maddox, S. 2004, MNRAS, 350, 398
- Larsen, S.S. & Richtler, T. 2000, A&A, 354, 836
- Lee, M.G., Kim, M., Sarajedini, A., Geisler, D. & Gieren, W. 2002, ApJ, 565, 959
- Lee, H., McCall, M.L., Kingsburgh, R.L., Ross, R., Stevenson, C.C. 2003, AJ, 125, 146
- Leonard, D.C., Filippenko, A.V., Gates, E.L., et al. 2002a, PASP, 114, 35
- Leonard, D.C., Filippenko, A.V., Li, W., et al. 2002b, AJ, 124, 2490
- Lequeux, J., Peimbert, M., Rayo, J.F., Serrano, A. & Torres-Peimbert, S. 1979, A&A, 80, 155
- Macri, L.M., Stetson, P.B., Bothun, G.D., et al. 2001, ApJ, 559, 243
- Magrini, L., Corradi, R.L.M., Mampaso, A. & Perinotto, M. 2000, A&A, 355, 713
- Malinie, G., Hartmann, D.H., Cayton, D.D. & Mathews, G.J. 1993, ApJ, 413, 633
- McCall, M.L., Rybski, P.M. & Shields G.A. 1985, ApJS, 57, 1
- McGaugh, S.S. 1991, ApJ, 380, 140
- Melbourne, J. & Salzer, J.J. 2002, AJ, 123, 2302
- Melbourne, J., Phillips, A., Salzer, J.J., Gronwall, C. & Sarajedini, V.L. 2004, AJ, 127, 686
- Meyer, D.M., Jura, M. & Cardelli, J.A. 1998, ApJ, 493, 222
- Milliard, B. & Marcelin, M. 1981, A&A, 95, 59
- Mollá, M., Ferrini, F. & Díaz, A.I. 1996, ApJ, 466, 668
- Mollá, M., Ferrini, F. & Díaz, A.I. 1997, ApJ, 475, 519
- Mouhcine, M. & Contini, T. 2002, A&A, 389, 106
- Mould, J., Aaronson, M. & Huchra, J. 1980, ApJ, 238, 458
- Mould, J. & Kristian, J. 1986, ApJ, 305, 591
- Newman, J.A., Ferrarese, L., Stetson, P.B., et al. 2001, ApJ, 553, 562
- Nishiyama, K. & Nakai, N. 2001, PASJ, 53, 713
- Nishiyama, K., Nakai, N. & Kuno, N. 2001, PASJ, 53, 757
- Ondrechen, M.P. & van der Hulst, J.M. 1989, ApJ, 342, 29
- Oey, M.S. & Kennicutt, R.C. 1993, ApJ, 411, 137
- Pagel, B.E.J. 2003, in *CNO in the Universe*, Eds. C. Charbonnel, D. Schaerer & G. Meynet, ASP Conference Series, v. 304, p. 187
- Pagel, B.E.J., Edmunds, M.G., Blackwell, D.E., Chun, M.S. & Smith, G. 1979, MNRAS, 189, 95
- Pagel, B.E.J., Simonson, E.A., Terlevich, R.J. & Edmunds, M.G. 1992, MNRAS, 255, 325
- Pagel, B.E.J. & Tautvaišienė, G. 1995, MNRAS, 276, 505
- Parodi, B.R., Saha, A., Sandage, A. & Tammann, G.A. 2000, ApJ, 540, 634
- Paturel, G. 1984, ApJ, 282, 382
- Paturel, G., Lanoix, P., Teerikorpi, P., et al. 1998, A&A, 339, 671
- Peimbert, M. 1970, PASP, 82, 636
- Peterson, C.J. 1978, ApJ, 226, 75
- Pierce, M.J. 1994, ApJ, 430, 53
- Pierce, M.J., McClure, R.D. & Racine, R. 1992, ApJ, 393, 523
- Pierce, M.J. & Tully, R.B. 1988, ApJ, 330, 579
- Pilyugin, L.S., 2000, A&A, 362, 325
- Pilyugin, L.S., 2001a, A&A, 369, 594
- Pilyugin, L.S., 2001b, A&A, 373, 56
- Pilyugin, L.S., 2001c, A&A, 374, 412
- Pilyugin, L.S., 2003a, A&A, 397, 109
- Pilyugin, L.S., 2003b, A&A, 399, 1003
- Pilyugin, L.S. & Edmunds, M.G. 1996a, A&A, 313, 792
- Pilyugin, L.S. & Edmunds, M.G. 1996b, A&A, 313, 803
- Pilyugin, L.S. & Ferrini, F. 1998, A&A, 336, 103
- Pilyugin, L.S. & Ferrini, F. 2000a, A&A, 354, 874
- Pilyugin, L.S. & Ferrini, F. 2000b, A&A, 358, 72
- Pilyugin, L.S., Ferrini, F., Shkvarun, R.V., 2003, A&A, 401, 557
- Pilyugin, L.S., Mollá, M., Ferrini, F. & Vílchez, J.M. 2002, A&A, 383, 14
- Pilyugin, L.S., Thuan, T.X. & Vílchez, J.M. 2003, A&A, 397, 487
- Puche, D., Carignan, C. & Bosma, A. 1990, AJ, 100, 1468
- Puche, D., Carignan, C. & van Gorkom, J.H. 1991, AJ, 101, 456
- Rayo, J.F., Peimbert, M. & Torres-Peimbert, S. 1982, ApJ, 255, 1
- Reakes, M. 1979, MNRAS, 187, 525
- Richer, M.G. & McCall, M.L. 1995, ApJ, 445, 642
- Reif, K., Mebold, U., Goss, W.M., van Woerden, H. & Siegmán, B. 1982, A&AS, 50, 451
- Rodríguez, M. 1999, A&A, 351, 1075

- Rogstad, D.H., Crutcher, R.M. & Chu, K. 1979, *ApJ*, 229, 509
- Rothberg, B., Saunders, W., Tully, R.B. & Witchalls, P.L. 2000, *ApJ*, 533, 781
- Rots, A.H. 1975, *A&A*, 45, 43
- Rots, A.H. 1980, *A&AS*, 41, 189
- Roy, J.-R. & Walsh, J.R. 1997, *MNRAS*, 288, 715
- Rubin, V.C., Ford, W.K. & Thonnard, N. 1980, *ApJ*, 238, 471
- Russell, D.G. 2002, *ApJ*, 565, 681
- Ryder, S.D. 1995, *ApJ*, 444, 610
- Ryder, S.D., Koribalski, B., Staveley-Smith, L., et al. 2001, *ApJ*, 555, 232
- Sage, L.J. 1993, *A&A*, 272, 123
- Saha, A., Claver, J. & Hoessel, J.G. 2002, *AJ*, 124, 839
- Saikia, D.J., Pedlar, A., Unger, S.W. & Axon, D.J., 1994, *MNRAS*, 270, 46
- Sandqvist, A., Jörsäter, S. & Lindblad, P.O. 1995, *A&A*, 295, 585
- Schmidt, B.P., Kirshner, R.P., Eastman, R.G., et al. 1994, *ApJ*, 432, 42
- Schneider, S.E. 1989, *ApJ*, 343, 94
- Schöniger, F. & Sofue, Y. 1994, *A&A*, 283, 21
- Schöniger, F., & Sofue, Y. 1997, *A&A*, 323, 14
- Searle, L. 1971, *ApJ*, 168, 327
- Shanks, T. 1997, *MNRAS*, 290, L77
- Shapley, A., Fabbiano, G. & Eskridge, P.B. 2001, *ApJS*, 137, 139
- Sharina, M.E., Karachentsev, I.D. & Tikhonov, N.A. 1996, *A&AS*, 119, 499
- Sharina, M.E., Karachentsev, I.D. & Tikhonov, N.A. 1997, *PAZh*, 23, 373
- Shields, G.A. & Searle, L. 1978, *ApJ*, 222, 821
- Shields, G.A., Skillman, E.D. & Kennicutt, R.C. 1991, *ApJ*, 371, 82
- Shostak, G.S. 1978, *A&A*, 68, 321
- Skillman, E.D., Kennicutt, R.C. & Hodge, P.W. 1989, *ApJ*, 347, 875
- Skillman, E.D., Kennicutt, R.C., Shields, G.A. & Zaritsky, D. 1996, *ApJ*, 462, 147
- Skillman, E.D., Terlevich, R., Teuben, P.J. & van Woerden, H. *A&A*, 198, 33
- Smith, H.E. 1975, *ApJ*, 199, 591
- Soffner, T., Méndez, R.H., Jacoby, G.H., et al. 1996, *A&A*, 306, 9
- Sofia, U.J. & Meyer, D.M. 2001, *ApJL*, 554, L221
- Sohn, Y.-J. & Davidge, T.J. 1996, *AJ*, 111, 2280
- Sohn, Y.-J. & Davidge, T.J. 1998, *AJ*, 115, 130
- Solanes, J.M., Sanchis, T., Salvador-Solé, E., Giovanelli, R. & Haynes, M.P. 2002, *AJ*, 124, 2440
- Sorai, K., Nakai, N., Kuno, N., Nishiyama, K. & Hasegawa, T. 2000, *PASJ*, 52, 785
- Sperandio, M., Chincarini, G., Rampazzo, R. & de Souza, R. 1995, *A&AS*, 110, 279
- Stark, A.A., Elmegreen, B.G. & Chance, D. 1987, *ApJ*, 322, 64
- Stark, A.A., Knapp, G.R., Bally, J., et al. 1986, *ApJ*, 310, 660
- Staveley-Smith, L. & Davies, R.D. 1988, *MNRAS*, 231, 833
- Stauffer, J.R. & Bothun, G.D. 1984, *AJ*, 89, 1702
- Takamiya, T. & Sofue, Y. 2000, *ApJ*, 534, 670
- Terry, J.N., Paturel, G. & Ekholm, T. 2002, *A&A*, 393, 57
- Thim, F., Tammann, G.A., Saha, A., et al. 2003, *ApJ*, 590, 256
- Thornley, M.D. & Mundy, L.G. 1997, *ApJ*, 484, 202
- Tikhonov, N.A., Galazutdinova, O.A. & Drozdovsky, I.O. 2000, *Afz*, 43, 367
- Tonry, J.L., Dressler, A., Blakeslee, J.P., et al. 2001, *ApJ*, 546, 681
- Torres-Peimbert, S., Peimbert, M. & Fierro, J. 1989, *ApJ*, 345, 186
- Tosi, M. 1988a, *A&A*, 197, 33
- Tosi, M. 1988b, *A&A*, 197, 47
- Tully, R.B. 1988, *Nearby Galaxies Catalogue* (Cambridge: Cambridge Univ. Press)
- Tully, R.B. & Pierce, M.J., 2000, *ApJ*, 533, 744
- Tutui, Y. & Sofue, Y. 1997, *A&A*, 326, 915
- Tutui, Y. & Sofue, Y. 1999, *A&A*, 351, 467
- van Albada, T.S., Bahcall, J.N., Begeman, K. & Sancisi, R. 1985, *ApJ*, 295, 305
- van Albada, G.D. & Shane, W.W. 1975, *A&A*, 42, 433
- van der Kruit, P.C. & Shostak, C.S. 1984, *A&A*, 134, 258
- van Zee, L. & Bryant, J. 1999, *AJ*, 118, 2172
- van Zee, L., Salzer, J.J., Haynes, M.P., O'Donoghue, A.A. & Balonek T.J. 1998, *AJ*, 116, 2805
- Verdes-Montenegro, L., Bosma, A. & Athanassoula, E. 2000, *A&A*, 356, 827
- Vila-Costas, M.B. & Edmunds, M.G. 1992, *MNRAS*, 259, 121
- Vílchez, J.M., Edmunds, M.G. & Pagel, B.E.J. 1988, *PASP*, 100, 1428
- Vílchez, J.M., Pagel, B.E.J., Díaz, A.I., Terlevich, E. & Edmunds M.G. 1988, *MNRAS*, 235, 633
- Warmels, R.H. 1988a, *A&AS*, 72, 19
- Warmels, R.H. 1988b, *A&AS*, 72, 57
- Webster, B.L. & Smith, M.G. 1983, *MNRAS*, 204, 743
- Weliachew, L. & Gottesman, S.T. 1973, *A&A*, 24, 59
- Wevers, B.M.H.R., Appleton, P.N., Davies, R.D. & Hart, L. 1984, *A&A*, 140, 125
- Wevers, B.M.H.R., van der Kruit, P.C. & Allen, R.J. 1986, *A&AS*, 66, 505
- Wilcots, E.M. & Miller, B.W. 1998, *AJ*, 116, 2363
- Yasuda, N., Fukugita, M. & Okamura, S. 1997, *ApJS*, 108, 417
- Young, J.S., Xie, S., Tacconi, L., et al. 1995, *ApJS*, 98, 219
- Zaritsky, D., Kennicutt, R.C. & Huchra, J.P. 1994, *ApJ*, 420, 87

Appendix A: Distances and luminosities

To derive a reliable galaxy luminosity, an accurate value of the distance is necessary. Over the past decade, great progress has been made in accurate distance measurements for galaxies using many different methods. Therefore, we have performed a thorough literature search for distance information to determine the most reliable, up-to-date distances for our sample.

The Cepheid period–luminosity relation remains the most useful method for estimating the distance of galaxies. Another efficient tool is the luminosity of the tip of the red giant branch (TRGB) stars. One of the most promising distance indicators is believed to be the peak brightness of type Ia supernovae (SNe Ia). The supernovae of type II (SNe II) are also reliable distance indicators; the method of distance determination is based on models of the expanding photospheres of SNe II (EPM). The planetary nebula luminosity function (PNLF) is a reliable distance indicator for galaxies potentially as far away as ~ 25 Mpc. Surface brightness fluctuations (SBF) have emerged

as a reliable distance indicator. The classic method of distance measurements via the luminosity of the brightest blue and red supergiants (BBSG and BRSG) has been widely used over last decade. The Tully-Fisher (TF) relation, or “luminosity–rotation velocity” relation, is the most commonly applied distance indicator for spiral galaxies at the present time. There are different versions of the TF relation: the luminosity in different bands can be used in the TF relation, and the CO linewidth instead of the H I linewidth can be used as the tracer of rotation velocity.

The important point is that the TRGB, SNIa, PNLF, SBF, BRSG, and TF methods request a calibration. The *Hubble Space Telescope* Key Project on the Extragalactic Distance Scale has provided Cepheid distances to more than 20 galaxies, in addition to the existing ground-based Cepheid distances to about 10 galaxies. This data set constitutes a solid basis for calibrating other distance indicators (Ferrarese et al. 2000). It should be noted, however, that some uncertainty in the Cepheid distances still remains, due to uncertainties in the slope and zero point of the Cepheid period – luminosity relation (see discussion in Ferrarese et al. 2000; Freedman et al. 2001; among others). Therefore, the slightly different values of the Cepheid distance to a given galaxy have been derived by different authors using the same observational data. As a result, there is some disagreement in the literature on the magnitudes of other standard candles. For example, two recent calibrations of the peak absolute magnitude of SNe Ia, based on the SNe Ia events in galaxies with known Cepheid distances result in slightly different magnitudes: $M_B = -19.56$ (Parodi et al. 2000) and $M_B = -19.32$ (Gibson & Stetson 2001). The method based on modeling the expanding photospheres of SNe II is a “physical method” and is hence completely independent of the calibration of the local distance scale. The EPM distances agree with the Cepheid distances within around 10% (Eastman, Schmidt & Kirshner 1996; Leonard et al. 2002a). Since systematic uncertainty clearly remains at the 10% level for Cepheid and at the 10–20% level for EPM, it is not clear whether the observed discrepancy is significant (Leonard et al. 2002a).

The most important point to take into account when comparing different methods of distance determination is their accuracy. The *relative* Cepheid distances are determined to $\sim \pm 5\%$ (Freedman et al. 2001). A typical accuracy of the TRGB distances is $\sim 12\%$ (Karachentsev et al. 2003a, b). According to Parodi et al. (2000), the SNe Ia are the best standard candles known so far, with a luminosity scatter of less than 0.25 mag. The EPM distances agree with the Cepheid distances within $\sim 10\%$ (Eastman, Schmidt & Kirshner 1996; Leonard et al. 2002a). There is also a good agreement between PNLF and Cepheid distances over two orders of magnitude in the derived distances (Feldmeier, Ciardullo & Jacoby 1997). The SBF distance measurements rely on the empirical calibration of absolute fluctuation amplitudes. A relative accuracy of $\sim 10\%$ in extragalactic SBF distances can be reached, provided that the galaxy color is well known (Jensen et al.

2003). Distance moduli derived with the BBSG and BRSG method have typical errors of 0.4 – 0.5 mag (Drozdovsky & Karachentsev 2000). Solanes et al. (2002) have examined the TF distance moduli of spiral galaxies in the region of the Virgo cluster taken from eight published datasets and have found a dispersion of 0.41 mag. Tutui & Sofue (1997, 1999) have analysed H I and CO TF methods. They concluded that the errors in the H I TF distances can be especially large in the case of interacting galaxies since the H I linewidth may be strongly disturbed by galaxy – galaxy interaction and may not reflect correctly the rotation velocity of the galaxy. The method of “sosie galaxies” (look-alike galaxies) is a particular application of the TF method which avoids some practical problems (Paturel 1984; Terry, Paturel & Ekholm 2002). The distances derived with the “sosie galaxies” method appear to be more reliable than those obtained with the direct TF relation.

Typically, two or more distance estimations for a galaxy from our sample are available in the literature. Examination of available distances confirms that the Cepheid, EPM, SBF, SNIa, PNLF, and TRGB methods provide accurate distance determinations. Estimations of distances with two or more of these methods exist for 14 galaxies from our sample. The deviation of individual distance estimations from the mean value is usually less than 10%. These methods will be referred to as “high-precision” methods below. The agreement between the TF (and BBSG, BRSG) distances and distances derived with the high-precision methods is appreciably worse. Moreover, the TF distances derived by different authors for the same galaxy can show a significant scatter. Taking these facts into account, the adopted value of the distance for a galaxy is chosen in the following way. If the distance derived with the “high-precision” method(s) is available, this distance is adopted. If only the TF and/or BBSG, BRSG distances are available, the mean value is adopted. If a galaxy is a member of compact group, the information on the distances to other members of the group is used to check the distance. We have to adopt the redshift (H_0) distances for three galaxies (NGC3344, NGC5068, and IC5201) from our sample due to the lack of other reliable distance estimations.

Here are some comments on individual galaxies.

NGC628. – There is no distance to NGC628 determined with one of the “high-precision” methods. However, the available distances to NGC628 derived with the method of brightest stars seem to be quite reliable. Firstly, the distances derived from two different investigations are in agreement: 7.24 Mpc (Sohn & Davidge 1996) compared to 7.32 Mpc (Sharina, Karachentsev & Tikhonov 1996). Secondly, the distance moduli estimated by Sharina, Karachentsev & Tikhonov (1996) for four galaxies in the group of NGC628 have a mean value of 7.80 Mpc with a small scatter. As noted by Sharina, Karachentsev & Tikhonov (1996), if a group contains a sufficient number of irregular galaxies, the “brightness stars” method makes it possible to measure the distance

Table A.1. The general properties of spiral galaxies from our sample

galaxy	T-Type	morphology	B_T^0	$\log L_B$ (L_\odot)	distance Mpc	references for distance values
NGC224 = M31	3.0	SA(s)b	3.36	10.63	0.78	FMG01, JPN03, MK86, JTB03, TDB01, SS94
NGC253	5.0	SAB(s)c	7.09	10.55	3.94	KSD03, TS00
NGC300	7.0	SA(s)d	8.49	9.40	2.00	FMG01, SMJ96
NGC598 = M33	6.0	SA(s)cd	5.75	9.74	0.84	FMG01, TS00, MCM00, LKS02, KKL02
NGC628 = M74	5.0	SA(s)c	9.76	10.01	7.28	SD96, SKT96, HFS97
NGC753	4.0	SAB(rs)bc	12.35	10.64	49.30	R02
NGC925	7.0	SAB(s)d	9.97	10.13	9.16	FMG01, SD98, TPE02
NGC1058	5.0	SA(rs)c	11.55	9.62	10.60	SKE94, TPE02
NGC1068 = M77	3.0	(R)SA(rs)b	9.47	10.77	15.30	SS94, TS00, HFS97
NGC1232	5.0	SAB(rs)c	10.38	10.55	17.90	R02, TPE02
NGC1365	3.0	(R)SBb(s)c	9.93	10.73	17.95	FMG01, SS94
NGC2403	6.0	SAB(s)cd	8.43	9.84	3.22	FMG01, CFJ02
NGC2442	3.7	SAB(s)bc	10.36	10.72	21.58	RKS01, TDB01
NGC2541	6.0	SA(s)cd	11.57	9.66	11.22	FMG01, HFS97
NGC2805	7.0	SAB(rs)d	11.17	9.70	9.77	TDB01
NGC2835	5.0	SAB(rs)c	10.31	10.05	9.80	R02, TDB01
NGC2841	3.0	SA(r)b	9.58	10.66	14.06	MSB01, HFS97
NGC2903	4.0	SB(s)d	9.11	10.44	8.87	DK00, TPE02, TS00
NGC2997	5.0	SA(s)c	9.34	10.46	10.05	R02, SPU94, T88, V79
NGC3031 = M81	2.0	SA(s)ab	7.39	10.36	3.63	FMG01, JCB89, JTB03, TDB01, TPE02
NGC3184	6.0	SAB(rs)cd	10.34	10.15	11.10	HFS97, LFL02, V79
NGC3198	5.0	SB(rs)c	10.21	10.39	13.80	FMG01, TPE02
NGC3344	4.0	(R)SAB(r)bc	10.50	9.67	6.90	VBA00
NGC3351 = M95	3.0	SB(r)b	10.26	10.09	10.00	CFJ02, FMG01, TPE02
NGC3521	4.0	SAB(rs)bc	9.29	10.49	10.21	HFS97, RST00, TS00
NGC3621	7.0	SA(s)d	9.20	10.16	6.64	FMG01, TPE02
NGC4254 = M99	5.0	SA(s)c	10.10	10.57	16.14	R02, SS97, SSS02
NGC4258 = M106	4.0	SAB(s)bc	8.53	10.58	7.98	CFJ02, CMM02, FMG01, HMG99, NFS01
NGC4303 = M61	4.0	SAB(rs)bc	10.12	10.10	9.55	SPU94, SS97, TS00
NGC4321 = M100	4.0	SAB(s)bc	9.98	10.56	15.21	FMG01, R02, SKE94, SSS02, TPE02, TS00
NGC4395	9.0	SA(s)m	10.57	9.29	4.61	HFS97, KMS03, KD98
NGC4501 = M88	3.0	SA(rs)b	9.86	10.74	17.58	R02, SS97, SSS02
NGC4559	6.0	SAB(rs)cd	9.76	9.90	6.40	HFS97, RST00
NGC4571	6.5	SA(r)d	11.73	9.97	17.22	PMR92, SS97, SSS02, TGD00
NGC4651	5.0	SA(rs)c	11.04	10.47	22.28	SS97, SSS02, TPE02
NGC4654	6.0	SAB(rs)cd	10.75	10.17	13.74	SS97, SSS02
NGC4689	4.0	SA(rs)bc	11.39	9.99	15.00	SS97, SSS02
NGC4713	7.0	SAB(rs)d	11.85	9.72	13.61	SSS02
NGC4725	2.0	SAB(r)ab	9.78	10.46	12.36	JTB03, FMG01, TDB01, TPE02
NGC4736 = M94	2.0	(R)SA(r)ab	8.75	10.08	4.93	KMS03, SS94, TDB01, TPE02, TS00
NGC5033	5.0	SA(s)c	10.21	10.51	15.82	RST00, SFE01, TPE02
NGC5055 = M63	4.0	SA(rs)bc	9.03	10.47	8.81	RST00, TPE02, TS00
NGC5068	6.0	SB(s)d	10.09	9.70	5.90	SFE01
NGC5194 = M51	4.0	SA(s)bc	8.67	10.49	7.64	CFJ02, FCJ97, SS94, TDB01, TS00
NGC5236 = M83	5.0	SAB(s)c	7.98	10.30	4.49	ESK96, SKE94, TTS03
NGC5457 = M101	6.0	SAB(rs)cd	8.21	10.56	6.70	DK00, FCJ97, FMG01, JPJ00, SKE94
NGC6384	4.0	SAB(r)bc	10.60	10.79	26.14	P94, PSS00, S97, TPE02
NGC6744	4.0	SAB(r)bc	8.82	10.60	9.33	SFE01, TPE02
NGC6946	6.0	SAB(rs)cd	7.78	10.59	5.70	ESK96, SKE94, SKT97, SS94, TPE02, TS00
NGC7331	3.0	SA(s)b	9.38	10.78	14.72	FMG01, JTB03, SKE94, TDB01, TPE02
NGC7793	7.0	SA(s)d	9.37	9.63	3.91	KSD03, D98
IC342	6.0	SAB(rs)cd	6.04	10.81	3.28	KT93, SCH02, SS94, TS00
IC5201	6.0	SB(s)cd	11.00	9.87	11.00	T88

Table A.2. List of references to Table A.1

Abbreviation	Reference	Method
CFJ02	Ciardullo, Feldmeier, Jacoby, et al. 2002	PNLF
CMM02	Caputo, Marconi & Musella 2002	Cepheid
D98	Davidge 1998	BRSG
DK00	Drozdovsky & Karachentsev 2000	TRGB
ESK96	Eastman, Schmidt & Kirshner 1996	EPM
FCJ97	Feldmeier, Ciardullo & Jacoby 1997	PNLF
FMG01	Freedman, Madorw, Gibson, et al. 2001	Cepheid
HFS97	Ho, Filippenko & Sargent 1997	H ₀
HMG99	Herrnstein, Moran, Greenhil, et al. 1999	geometric
JCB89	Jacoby, Ciardullo, Booth, et al. 1989	PNLF
JPJ00	Jurcevic, Pierce & Jacoby 2000	RSGV
JPN03	Joshi, Pandey, Narasimha, et al. 2003	RSGV
JTB03	Jensen, Tonry, Barris, et al. 2003	SBF
KD98	Karachentsev & Drozdovsky 1998	BBSG
KKL02	Kim, Kim, Lee, et al. 2002	TRGB
KMS03	Karachentsev, Makarov, Sharina, et al. 2003a	TRGB
KSD03	Karachentsev, Sharina, Dolphin, et al. 2003b	TRGB
KT93	Karachentsev & Tikhonov 1993	BRGB
LFL02	Leonard, Filippenko, Li, et al. 2002b	EPM
LKS02	Lee, Kim, Sarajedini, et al. 2002	Cepheid
MCM00	Magrini, Corradi, Mampaso, et al. 2000	PNLF
MK86	Mould & Kristian 1986	TRGB
MSB01	Macri, Stetson, Bothun, et al. 2001	Cepheid
NFS01	Newman, Ferrarese, Stetson, et al. 2001	Cepheid
P94	Pierce 1994	SNIa
PMR92	Pierce, McClure & Racine 1992	BRSG
PSS00	Parodi, Saha, Sandage, et al. 2000	SNIa
R02	Russel 2002	TF
RKS01	Ryder, Koribalski, Staveley-Smith, et al. 2001	H ₀
RST00	Rothberg, Saunders, Tully, et al. 2000	H ₀
S97	Shanks 1997	SNIa
SCH02	Saha, Claver & Hoessel 2002	Cepheid
SD96	Sohn & Davidge 1996	BRSG
SD98	Sohn & Davidge 1998	BRSG
SFE01	Shapley, Fabbiano & Eskridge 2001	H ₀
SKE94	Schmidt, Kirshner, Eastman, et.al. 1994	EPM
SKT96	Sharina, Karachentsev & Tikhonov 1996	BBSG
SKT97	Sharina, Karachentsev & Tikhonov 1997	BBSG
SMJ96	Soffner, Méndez, Jacoby, et al. 1996	BBSG
SPU94	Saikia, Pedlar, Unger, et al. 1994	H ₀
SS94	Schöniger & Sofue 1994	TF
SS97	Schöniger & Sofue 1997	TF
SSS02	Solanes, Sanchis, Salvador, et.al. 2002	TF
T88	Tully 1988	H ₀
TDB01	Tonry, Dressler, Blakeslee, et al. 2001	SBF
TGD00	Tikhonov, Galazutdinova & Drozdovsky 2000	BSG
TPE02	Terry, Paturel & Ekholm 2002	sosie(TF)
TS00	Takamiya & Sofue 2000	TF
TTS03	Thim, Tammann, Saha, et al. 2003	TF
V79	de Vaucouleurs 1979	tertiary
VBA00	Verdes-Montenegro, Bosma & Athanassoula 2000	H ₀

to the group with almost the same accuracy as with the Cepheid method.

NGC753. – The galaxy NGC753 belongs to the Pisces filament. The TF distances of several dozens of galaxies of this filament lie between ~ 50 Mpc and ~ 80 Mpc (Tully & Pierce 2000). The TF distance (49.30 Mpc) of NGC753 from Russel (2002) is adopted here.

NGC1068. – Two values of TF distances to NGC1068 show an appreciable discrepancy: 12.45 Mpc (Schöniger & Sofue 1994) compared with 18.10 Mpc (Takamiya & Sofue 2000). The galaxy NGC1068 is a member of the LGG73 group (Garcia 1993). A distance of 16.07 Mpc to the galaxy NGC1055 (also a member of LGG73 group) was estimated by Paturel et al. (1998) using the method of “sosies galaxies”. The mean TF distance of 15.30 Mpc is confirmed by the Paturel et al.’s data and is adopted here.

NGC2442. – There is no reliable distance determination for NGC2442. This galaxy is a member of the LGG147 group (Garcia 1993). The distance to another member (NGC2434) of this group has been determined with the SBF method and is equal to 21.58 Mpc (Tonry et al. 2001). This value is adopted as distance to NGC2442.

NGC2805. – There is no reliable distance determination for NGC2805. This galaxy is a member of the LGG173 group (Garcia 1993). The distance to another member (NGC2880) of this group has been determined with the SBF method and is equal to 9.77 Mpc (Tonry et al. 2001). This value is adopted as distance to NGC2805.

NGC2835. – Different distance values to NGC2835 were used recently: 10.76 Mpc (Elmegreen & Salzer 1999) and 6.03 Mpc (Larsen & Richtler 2000). The TF distance to NGC2835 is 9.80 Mpc (Russel 2002). The galaxy NGC2835 is a member of the LGG172 group (Garcia 1993). The distance to NGC2784 (a member of the LGG172 group) has been determined with the SBF method and is equal to 9.82 Mpc (Tonry et al. 2001). This value is adopted as distance to NGC2835.

Virgo galaxies. – We chose individual distance estimations to Virgo galaxies in the same way as in the case of field galaxies. If the distance estimation with one of the “high-precision” methods is available, this distance is adopted. Otherwise the distance is derived by averaging the available TF distances. The distances of Virgo galaxies NGC4254, NGC4501, NGC4571, NGC4651, NGC4654, NGC4689, and NGC4713 were taken from Solanes et al. (2002). These distances were obtained by averaging distance moduli based upon the TF relationship taken from eight published datasets (Ekholm et al. 2000; Fouqué et al. 1990; Federspiel, Tammann & Sandage 1998; Gavazzi et al. 1999; Kraan-Korteweg, Cameron & Tammann 1988; Mould, Aaronson & Huchra 1980; Pierce & Tully 1988; Yasuda, Fukugita & Okamura 1997). The distances from these works have been previously homogenized. It seems quite impossible to check the distance of individual Virgo cluster galaxies by comparing their value with the “group” distance. Indeed, the galaxies NGC4321, NGC4651, and NGC4689 belong to the LGG289 group (Garcia 1993).

Their TF distances range from 15.00 Mpc for NGC4689 to 22.28 Mpc for NGC4651. The distances for nine galaxies of the LGG289 group have been determined with the SBF method (Tonry et al. 2001), these distances lie between 15.00 Mpc (NGC4564) and 22.42 Mpc (NGC4365). Thus, both the TF distances and the SBF distances of galaxies of LGG289 group are spread over more than 7 Mpc. There are two estimations of the distance to the Virgo cluster galaxy NGC4571 with the “brightest supergiant stars” method. The mean BRSG distance value of 17.15 Mpc is in agreement with Solanes et al.’s TF distance of 17.22 Mpc.

The adopted values of distance and the corresponding references to sources of data are presented in Table A.1 (Cols. 6 and 7). The list of references to Table A.1 is given in Table A.2. Using the adopted distances and the total face-on blue magnitudes corrected for galactic and internal absorption B_T^0 , the luminosities of galaxies were determined. The B_T^0 values are taken from the Third Reference Catalog of bright Galaxies (de Vaucouleurs et al 1991, RC3) and are listed in Col. 4 of Table A.1, the derived luminosities are given in Col. 5 of Table A.1.